International Journal of
Physical Sciences

ABOUT IJPS

The **International Journal of Physical Sciences (IJPS)** is published weekly (one volume per year) by Academic Journals.

International Journal of Physical Sciences (IJPS) is an open access journal that publishes high-quality solicited and unsolicited articles, in English, in all Physics and chemistry including artificial intelligence, neural processing, nuclear and particle physics, geophysics, physics in medicine and biology, plasma physics, semiconductor science and technology, wireless and optical communications, materials science, energy and fuels, environmental science and technology, combinatorial chemistry, natural products, molecular therapeutics, geochemistry, cement and concrete research, metallurgy, crystallography and computer-aided materials design. All articles published in IJPS are peer-reviewed.

Contact Us

Editors

International Journal of Physical Sciences

Table of Contents: Volume 13   Number 5,   16 March, 2018

ARTICLES

Full Length Research Paper

On the effect of convective heat and mass transfer on unsteady mixed convection MHD flow through vertical porous medium

M. M. Allan[1,2] and S. M. Dardery[1,2*]

[1]Department of Mathematics, Faculty of Sciences, Zagazig University, Zagazig, Egypt.
[2]Department of Mathematics, Faculty of Sciences and Art, Muthneb Quseem University, KSA.

In this paper, unsteady two-dimensional convective heat and mass transfer flow of a viscous, incompressible, electrically conducting optically thin fluid which is bounded by a vertical infinite plane surface was considered. A uniform applied homogeneous magnetic field is considered in the transverse direction with first order chemical reaction. An analytical solution for two-dimensional oscillatory flow on unsteady mixed convection of an incompressible viscous fluid, through a porous medium bounded by an infinite vertical plate in the presence of chemical reaction and thermal radiation are presented. The surface absorbs the fluid with a constant suction and the free stream velocity oscillates about a constant mean value. The resulting nonlinear partial differential equations were transformed into a set of ordinary differential equations using two-term series. The closed form solutions for velocity, temperature, concentration, skin friction, Nusselt number, and Sherwood number have been obtained, using the regular perturbation technique. Numerical evaluation of the analytical solutions was performed and the results are presented in tabular and graphical form. This illustrates the influence of the various parameters involved in the problem on the solutions.

Key words: Magnetohydrodynamics (MHD) flow, heat and mass transfer, oscillatory flow, thermal radiation, chemical reaction.

INTRODUCTION

The influence of magnetic field on viscous incompressible flow of electrically conducting fluid has its importance in many applications such as extrusion of plastics in the manufacture of rayon and nylon, purification of crude oil, pulp, paper industry, textile industry and in different geophysical cases, etc. The application of magnetohydrodynamics (MHD) flow is found in metrology, solar physics and in motion of earth's core. Also it has applications in the field of stellar and planetary magnetospheres, aeronautics, chemical engineering, and

electronics (Saxena et al., 2014; Rabi et al., 2013).

Oscillatory flows has been known to result in higher rates of heat and mass transfer, many studies have been done to understand its characteristics in different systems such as reciprocating engines, pulse combustors, and chemical reactors. The detailed study on fluid mechanics of oscillatory and modulated flows has been made by Cooper et al. (1993). The numerically studied influence of convective heat transfer from periodic open cavities in a channel with oscillatory flow has been studied by Fusegi (1997), Gomaa and Taweel (2005), and Abdelkader and Lounes (2007), respectively. The influence of MHD oscillatory flow on free convection radiation through a porous medium with constant suction velocity and the effect of slip condition on unsteady MHD oscillatory flow of a viscous fluid in a planer channel have been studied by El-Hakiem (2000), Makinde and Mhone (2005) and Mehmood and Ali (2007), respectively.

The MHD oscillatory flow past a vertical porous plate through porous medium in the presence of thermal and mass diffusion with constant heat source has been studied by Gholizadeh (1990). The work of Makinde (1994) is of particular interest since it demonstrated the possibility of achieving significant unsteady incompressible flow in a porous channel. The MHD mixed convection from a vertical plate embedded in porous medium with convective boundary condition has been analyzed by Makinde and Aziz (2010). Rabi et al. (2013) have investigated the influence of chemical reaction effect on MHD oscillatory flow through a porous medium bounded by two vertical porous plates with heat source Soret effect.

Chemical reactions are classified as either heterogeneous or homogeneous processes. These processes take place in numerous industrial applications, e.g., polymer production, manufacturing of ceramics and food processing (Cussler, 1998). The diffusion of chemically reactive species in a laminar boundary layer flow is analyzed by Chambre and Young (1958). The exact solution for hydrodynamic boundary layer flow and heat transfer is studied by Vajravelu (1986). Das et al. (1994), Muthucumaraswamy (2001, 2002) and Anjali Devi and Kandasamy (2002) studied the effect of a first-order chemical reaction on the flow in different cases. An analytical solution for heat and mass transfer by laminar flow of a Newtonian, viscous, and electrically conducting fluid is presented by Chamkha (2003). Kandasamy et al. (2005) studied the nonlinear MHD flow, with heat and mass transfer characteristics, of an incompressible, viscous, electrically conducting, Boussinesq fluid with chemical reaction and thermal stratification effects.

The role of thermal radiation is of major importance in engineering areas occurring at high temperatures and knowledge of radiative heat transfer becomes very important in nuclear power plants, gas turbines and the various propulsion devices for aircraft, missiles and space vehicles. Hakeem and Sathiyanathan (2009),

Srinivas and Muthuraj (2010), Pal and Talukdar (2010), Chamkha (2003), Bakr (2011) and Prakash et al. (2011) have examined the radiation effect of an oscillatory flow under different conditions. The influence of chemical reaction on unsteady MHD slip flow in a Planer channel with varying concentration has been examined by Sivaraj and Kumar (2011).

The main objective of this study is to investigate the effect of periodic heat and mass transfer on unsteady mixed convection MHD flow past an infinite vertical porous flat plate with constant suction in the presence of chemical reaction and thermal radiation when the free stream velocity is oscillating with time. The boundary layer equations governing the problem under consideration are solved by multi-parameter perturbation technique and giving more importance on analytic solution. For this study, air (*Pr=0.71*) and water (*Pr=6.2*) are the only fluids under consideration. The closed form solutions for velocity, temperature, skin friction, concentration, Nusselt number, and Sherwood number are presented. The effects of pertinent parameters on fluid flow of heat and mass transfer characteristics are studied in detail. This work is presented as follows. First, the problem is formulated and then the solution of the problem is presented. Following are the results and discussion, and finally, conclusions are summarized.

FORMULATION OF THE PROBLEM

Consider unsteady two-dimensional convective heat and mass transfer flow of a viscous, incompressible, electrically conducting optically thin fluid which is bounded by a vertical infinite plane surface. A uniform applied homogeneous magnetic field is considered from the transverse direction with first order chemical reaction. It was assumed that the surface absorbs the fluid with a constant velocity and the fluid far away the surface oscillates with time and assumed to be in the form $\bar{U}(t) = U_0(1 + \varepsilon e^{i\bar{\omega}t})$, where U_0 is the mean stream velocity and $\varepsilon(<<< 1)$ the amplitude of the free stream variation. A Cartesian coordinate system (x', y') is assumed, where x'- axis lies along the plate and y'- axis in the normal direction. Then, under the usual Boussinesq's approximation, the following equations governing the flow field are considered.

Continuity equation:

$$\frac{\partial v'}{\partial y'} = 0 \Rightarrow v' = -v_0 \tag{1}$$

Momentum equation:

$$\frac{\partial u'}{\partial t'} + v'\frac{\partial u'}{\partial y'} = -\frac{1}{\rho}\frac{\partial p'}{\partial x'} + \upsilon\frac{\partial^2 u'}{\partial y'^2} - \frac{\sigma B_0^2}{\rho}u' + g\beta(T' - T'_\infty) + g\beta_c(C' - C'_\infty) \tag{2}$$

Energy equation:

$$\frac{\partial T'}{\partial t'} + v'\frac{\partial T'}{\partial y'} = \frac{k}{\rho c_p}\frac{\partial^2 T'}{\partial y'^2} - \frac{1}{\rho c_p}\frac{\partial q_r}{\partial y'} \tag{3}$$

Concentration equation:

$$\frac{\partial C'}{\partial t'} + v'\frac{\partial C'}{\partial y'} = D\frac{\partial^2 C'}{\partial y'^2} - \gamma\left(C' - C'_\infty\right) \tag{4}$$

where (u', v') are velocity components in x' and y' directions, g is acceleration due to gravity, T' is the temperature of the fluid, C' is the species concentration, β is the coefficient of thermal expansion, β_c is the volumetric expansion coefficient, υ is the kinematic viscosity of the fluid, k is effective thermal conductivity, ρ is the density of the fluid, c_p is the specific heat at constant pressure, D is the diffusion coefficient, B_0 is the electromagnetic induction, σ is the conductivity of the fluid, v_0 constant suction/ injection and p is non-dimensional pressure.

The corresponding boundary conditions of the problem are:

$$u' = 0, \quad T' = T'_\omega + \left(T'_\omega - T'_\infty\right), \quad C' = C'_\omega + \varepsilon\left(C'_\omega - C'_\infty\right)e^{i\omega' t'} \, at \, y' = 0 \tag{5}$$

$$u' = U', \quad T' = T'_\infty, \quad C' = C'_\infty \qquad at \, y' \to \infty$$

And the radiative heat flux is given by

$$\frac{\partial q_r}{\partial y'} = 4\alpha^2\left(T'_0 - T'\right) \tag{6}$$

where $\alpha -$ is the radiation absorption coefficient .

Eliminating the modified pressure gradient under the usual boundary layer approximation (Equation 2) was reduced to

$$\frac{\partial u'}{\partial t'} + v'\frac{\partial u'}{\partial y'} = \frac{\partial U'}{\partial t'} + \upsilon\frac{\partial^2 u'}{\partial y'^2} - \frac{\sigma B_0^2}{\rho}\left(u' - U'\right) + g\beta\left(T' - T'_\infty\right) + g\beta_c\left(C' - C'_\infty\right) \tag{7}$$

introducing the following dimensionless quantities:

$$y = \frac{v_0}{\upsilon}y', \quad t = \frac{v_0^2}{\upsilon}t', \quad \omega = \frac{\upsilon\omega'}{v_0^2}, \quad u = \frac{u'}{U_0}, \quad U = \frac{U'}{U_0}, \tag{8}$$

$$\theta = \frac{T' - T'_\infty}{T'_w - T'}, \quad \phi = \frac{C' - C'_\infty}{C'_w - C'_\infty}, \quad k = \frac{v_0^2}{\upsilon^2}k'$$

With the help of the earlier non-dimensional variables,

Equations 1, 3, 4 and 7 were reduced to

$$\frac{\partial u}{\partial t} - \frac{\partial u}{\partial y} = \frac{\partial U}{\partial t} + \frac{\partial^2 u}{\partial y^2} + G_r\theta + G_c\phi + M\left(U - u\right) \tag{9}$$

$$\frac{\partial\theta}{\partial t} - \frac{\partial\theta}{\partial y} = \frac{1}{p_r}\frac{\partial^2\theta}{\partial y^2} + N\theta \tag{10}$$

$$\frac{\partial\phi}{\partial t} - \frac{\partial\phi}{\partial y} = \frac{1}{Sc}\frac{\partial^2\phi}{\partial y^2} - K_r\phi \tag{11}$$

The reduced boundary conditions are:

$$u = 0, \quad \theta = 1 + \varepsilon e^{i\omega t} \quad \phi = 1 + \varepsilon e^{i\omega t} \qquad at \, y = 0 \tag{12}$$

$$u = 1 + \varepsilon e^{i\omega t}, \quad \theta = 0, \quad \phi = 0 \qquad at \, y \to \infty$$

where $G_r = \dfrac{\upsilon g\beta}{U_0 v_0^2}\left(T_w - T_\infty\right)$ is Grashof number,

$G_c = \dfrac{\upsilon g\beta_c}{U_0 v_0^2}\left(C_w - C_\infty\right)$ is the modified Grashof

number, $M = \dfrac{\sigma B_0^2\upsilon}{\rho v_0^2}$ is magnetic number, $Sc = \dfrac{\upsilon}{D}$ is

the Schmidt number, $p_r = \dfrac{\rho\upsilon c_p}{k}$ is Prandtl number,

$K_r = \dfrac{\upsilon\gamma}{v_0^2}$ is the chemical reaction parameter and

$N = \dfrac{4\alpha^2\upsilon}{\rho c_p v_0^2}$ is radiation parameter.

METHOD OF SOLUTION

In order to solve the differential Equations 9, 10 and 11, we assume that:

$$u(y,t) = u_0(y) + \varepsilon e^{i\omega t}u_1(y),$$

$$\theta(y,t) = \theta_0(y) + \varepsilon e^{i\omega t}\theta_1(y), \tag{13}$$

$$\phi(y,t) = \phi_0(y) + \varepsilon e^{i\omega t}\phi_1(y)$$

where u_0, θ_0 and ϕ_0 are respectively the mean velocity, mean temperature and mean concentration. On using Equations 13 into 9, 10 and 11 and neglecting the higher order of ε, and simplifying we get the following set of equations:

$$\left[\frac{d^2}{dy^2} + \frac{d}{dy} - M\right]u_0 = -G_r\theta_0 - G_c\phi_0 - M \tag{14}$$

$$\left[\frac{d^2}{dy^2} + \frac{d}{dy} - M\right]\theta_0 = 0 \qquad (15)$$

$$\left[\frac{d^2}{dy^2} + \frac{d}{dy} - M\right]\phi_0 = 0 \qquad (16)$$

$$\left[\frac{d^2}{dy^2} + \frac{d}{dy} - M\right]u_1 = -G_r\theta_1 - G_c\phi_1 - (M + i\omega) \qquad (17)$$

$$\left[\frac{d^2}{dy^2} + p_r\frac{d}{dy} + p_r(N - i\omega)\right]\theta_1 = 0 \qquad (18)$$

$$\left[\frac{d^2}{dy^2} + Sc\frac{d}{dy} + Sc(K_r + i\omega)\right]\phi_1 = 0 \qquad (19)$$

The corresponding reduced boundary conditions are

$$u_0 = 0, \, u_1 = 0, \quad \theta_0 = 1, \, \theta_1 = 1, \, \phi_0 = 1, \, \phi_1 = 1 \, at \, y = 0 \quad (20)$$

$$u_0 = 1, \, u_1 = 1, \quad \theta_0 = 0, \, \theta_1 = 0, \, \phi_0 = 0, \, \phi_1 = 0 \, at \, y \to \infty$$

Solving Equations 14 into 19 with the conditions in Equation 20, we get:

$$u = -A_1 e^{m_1 y} - A_2 e^{m_2 y} + (A_1 + A_2 - 1)e^{m_3 y} + 1 +$$
$$\varepsilon e^{i\omega t}\left(-A_3 e^{m_4 y} - A_4 e^{m_5 y} + (A_3 + A_4 - 1)e^{m_6 y} + 1\right) \qquad (21)$$

$$\theta = e^{m_1 y} + \varepsilon e^{i\omega t}e^{m_4 y}, \qquad (22)$$

$$\phi = e^{m_2 y} + \varepsilon e^{i\omega t}e^{m_5 y}, \qquad (23)$$

where

$$m_1 = \frac{-pr - \sqrt{pr^2 - 4prN^2}}{2},$$

$$m_2 = \frac{-Sc - \sqrt{Sc^2 + 4Sckr}}{2},$$

$$m_3 = \frac{-1 - \sqrt{1 + 4M}}{2},$$

$$m_4 = \frac{-pr - \sqrt{pr^2 - 4pr(N^2 - i\omega)}}{2},$$

$$m_5 = \frac{-Sc - \sqrt{Sc^2 + 4Sc(kr + i\omega)}}{2},$$

$$m_6 = \frac{-1 - \sqrt{1 + 4(M + i\omega)}}{2},$$

$$A_1 = \frac{G_r}{m_1^2 + m_1 - M},$$

$$A_2 = \frac{G_c}{m_2^2 + m_2 - M},$$

$$A_3 = \frac{G_r}{m_4^2 + m_4 - (M + i\omega)},$$

$$A_2 = \frac{G_c}{m_5^2 + m_5 - (M + i\omega)},$$

The local skin friction coefficient, local Nusselt number and local Sherwood number are important physical quantities for this type of heat and mass transfer problem. They are defined as the following.

The dimensionless shearing stress on the surface of a body is written as:

$$\tau'_\omega = \mu\frac{\partial u'}{\partial y'}\bigg|_{y'=0} \qquad (24)$$

There, the local skin-friction factor is given by:

$$C_f = \frac{2\tau'_\omega}{\rho U_0 V_0} = 2\frac{\partial u}{\partial y}\bigg|_{y=0} \qquad (25)$$

The rate of heat transfer at the surface in terms of the local Nusselt number can be written as:

$$Nu = \frac{x}{T_\infty - T_\omega}\frac{\partial T'}{\partial y'}\bigg|_{y=0} \qquad (26)$$

$$Nu \, Re_x^{-1} = -\frac{\partial \theta}{\partial y}\bigg|_{y=0} \qquad (27)$$

where $Re_x^{-1} = -\frac{xV_0}{\upsilon}$ is the local Reynolds number.

The rate of heat transfer at the surface in terms of the local Sherwood number can be written as:

$$Sh = \frac{x}{C_\infty - C_\omega}\frac{\partial C'}{\partial y'}\bigg|_{y=0}$$

$$Sh \, Re_x^{-1} = -\frac{\partial \phi}{\partial y}\bigg|_{y=0} \qquad (28)$$

RESULTS AND DISCUSSION

Numerical evaluation of the analytical solutions reported in the previous section was performed and the results are presented in graphical and tabular form. This was done to illustrate the influence of the various parameters involved in the problem on the solutions in plotting the results.

The values of Grashof number G_r have been chosen as they are interesting from physical point of view. The free convection currents are due to temperature difference $T_m - T_\infty$ and hence $G_r > 0$ when $T_m - T_\infty > 0$ which physically corresponding to cooling of the plate by free-convection current, $G_r < 0$ corresponds to heating of the boundary surface by free-convection currents as $T_m - T_\infty < 0$ and $G_r = 0$ corresponds to the absence of free convection currents.

Figure 1 demonstrates the variation of the velocity distribution with the chemical reaction in the cases of cooling $(G_r > 0)$ and heating $(G_r < 0)$ by free convection currents. It observed that the velocity in the cases of cooling and heating decreases near the boundary layer with an increases in the chemical reaction parameter K_r. Also, Figure 1 shows that the effects of heating the surface leads to a fall in the velocity inside the boundary layer while the effect of cooling by free convection current, $(G_r > 0)$ is to increase the velocity more than in the case of heating the surface.

Figures 2 and 3 show the effects of chemical reaction on the concentration profiles with two values of Grashof number $G_r = 2$ (cooling of the surface) and $G_r = -2$ (heating of the surface), respectively. An increase in the values of K_r from 1, 1.5, 2, 2.5, and 3 causes a significant decrease in concentration profiles throughout the concentration boundary layer in the case of cooling and heating of the surface by free convection current.

Figure 4 illustrates the influence of the magnetic parameter M on the velocity profiles with two values of $G_r = -2$ (heating of the surface) and $G_r = 2$ (cooling of the surface). Application of a transfer magnetic field to an electrically conducting fluid gives rise to a resistive-type force called the Lorentz force. This force has the tendency to slow down the motion of the fluid in the boundary layer. This is obvious from decreases in the velocity profiles. Moreover, the magnetic field is found to cause an over shoot in the velocity profiles (that is, the velocity profiles exceed the values at the edge of the momentum boundary layer) in the case of cooling of the surface. However, no overshoot is observed in the case of heating of the surface whatever the values of magnetic field parameter are. Also, the effect of the magnetic field is found to be more pronounced for the case of cooling of

the surface than for the case of heating of the surface.

Figures 5 and 6 show the effects of the Grashof number G_r on the velocity profiles in the case of air ($p_r = 0.71$) and water ($p_r = 6.2$). From these figures, it was observed that the effects of cooling by free convection currents occur when $G_r > 0$. The velocity increases inside the boundary layer as G_r increases. In addition the curves show that the peak value of the velocity increases rapidly near the surface as the Grashof number increases and then decays to the free-stream velocity in the two cases air and water. Also, Figures 5 and 6 show the effect of heating by free convection currents when $G_r < 0$. An increase in greater heating of the surface leads to a fall in the velocity in the two cases of air and water. Also, it was noticed that the effects of Grashof number are found to be more pronounced for the fluid with small Prandtl number.

It was observed that the velocity and concentration decrease as the Schmidt number Sc increases, noted in the two cases of Prandtl number Pr=0.71, 6.2 (air and water) (Figures 7 to 9).

Figure 10 depicts the velocity profile for different values of radiation parameter N in two cases of Prandtl number Pr=0.71, 6.2. It was observed that the velocity decreases as the radiation parameter N decreases, velocity distribution for various values of radiation parameter N in case of the Prandtl number Pr =0.71 has a clear impact but its effect did not have a clear impact in case of the Prandtl number Pr=6.2, so we zoomed in water case to clarify influence.

The temporal development of temperature with different values of time t is elucidated in Figure 11. It is clear that the velocity of the fluid decreases as time increases, which noted in the two cases of Prandtl number Pr =0.71, 6.2, this is more evident in the case of air than in water case. It illustrated that the influence of the various parameters involved in the problem on the velocity of the air is greater than the velocity of the water under the same conditions.

Tables 1 and 2 show the effects of variations of Grashof number, modified Grashof number, chemical reaction, Schmidt number, magnetic parameter, frequency of the fluid and radiation parameter on the coefficients of skin friction, heat transfer and mass transfer, respectively for $\omega t = \pi / 2$, $\varepsilon = 0.5$ in the two cases air and water, respectively. It is clear that as Grashof number, modified Grashof number, Schmidtnumber, magnetic parameter and radiation parameter increase, skin friction coefficient increases, while decreasing by increasing chemical reaction and frequency of the fluid. Nusselt number decreases as frequency of the fluid and radiation parameter increase and Sherwood number increases as the chemical reaction and Schmidt number increase, while decrease by increasing frequency of the fluid. On the other hand,

Figure 1. Velocity distribution for various values of Grashof number Gr and chemical reaction parameter k_r for $\omega = 10$, $\omega t = \pi/2$, $\varepsilon = 0.5$, $N = 0.2$, $M = 5$, $G_c = 5$, Pr = 0.71, Sc = 0.22.

Figure 2. Concentration distribution for various values and chemical reaction parameter k_r for $\omega = 10$, $\omega t = \pi/2$, $\varepsilon = 0.5$, $N = 0.2$, $M = 5$, $G_c = 5$, Pr = 0.71, Sc = 0.22.
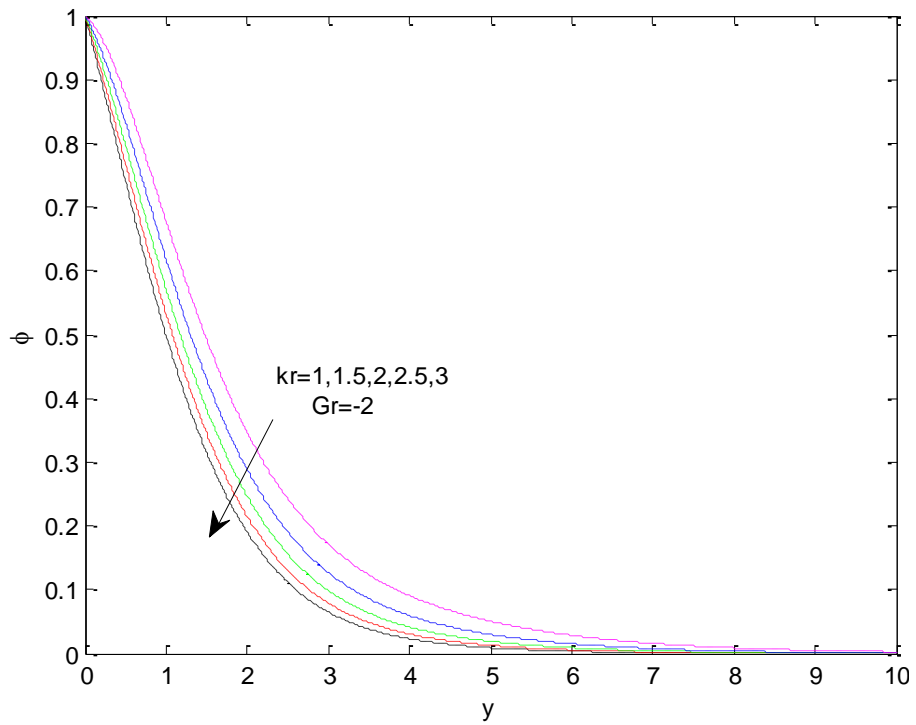
Figure 3. Concentration distribution for various values chemical reaction parameter k_r for $\omega = 10$, $\omega t = \pi/2$, $\varepsilon = 0.5$, $N = 0.2$, $M = 5$, $G_c = 5$, Pr = 0.71, $Sc = 0.22$.
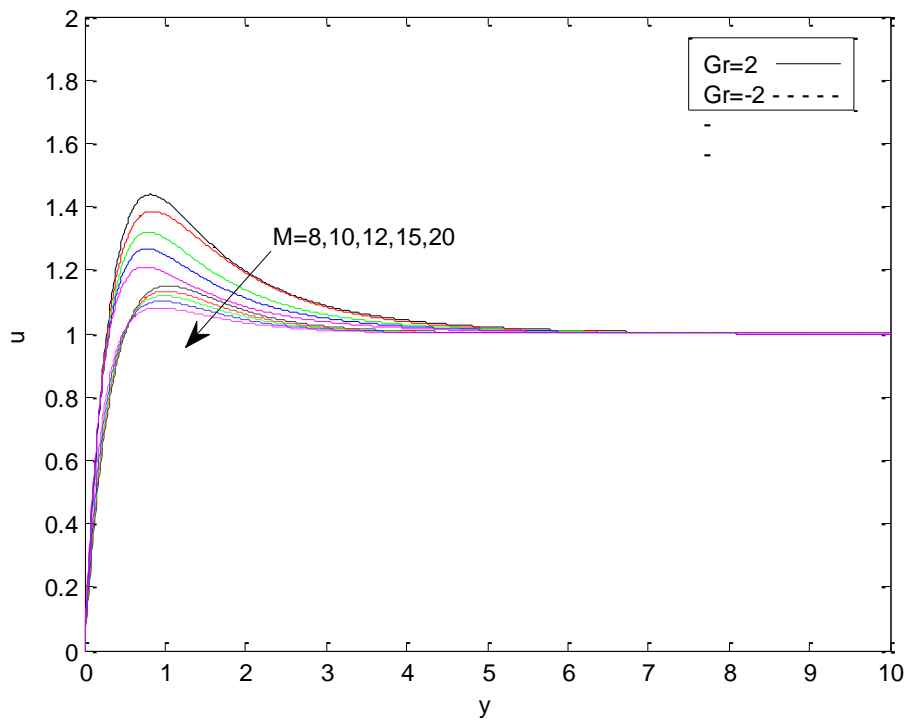
Figure 4. Velocity distribution for various values of Grashof number Gr and magnetic field parameter M for $\omega = 10$, $\omega t = \pi/2$, $\varepsilon = 0.5$, $N = 0.2$, $kr = 2$, $G_c = 5$, pr=0.71, $Sc = 0.22$
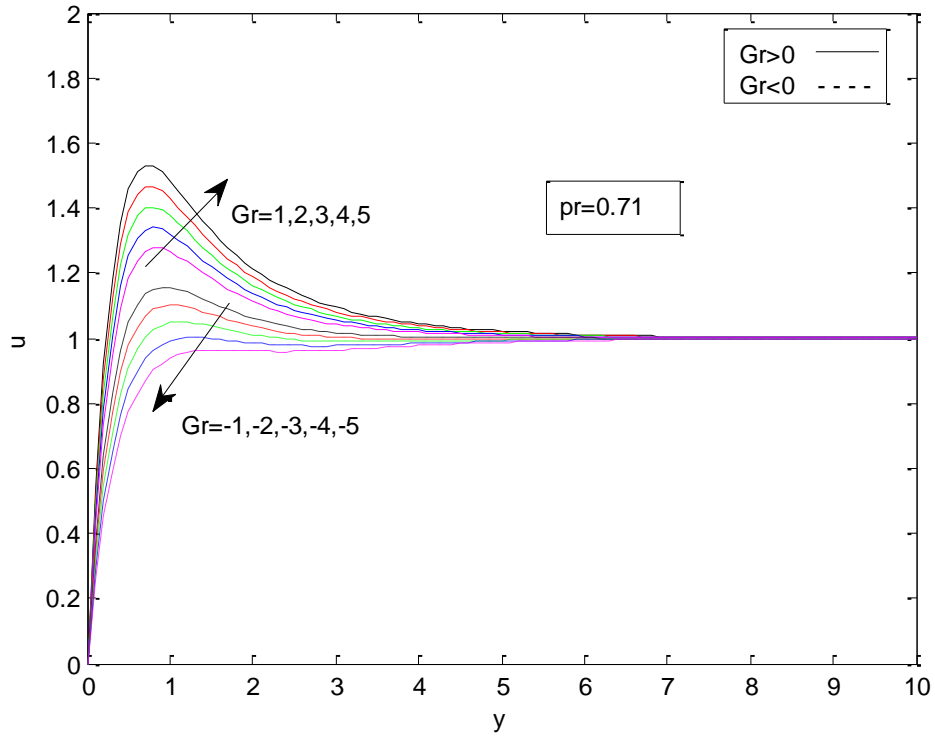
Figure 5. Velocity distribution for various values of Grashof number Gr for $\omega = 10$, $\omega t = \pi/2$, $\varepsilon = 0.5$, $N = 0.2$, $M = 10$, $G_c = 5$, $kr = 3$, $Sc = 0.22$.
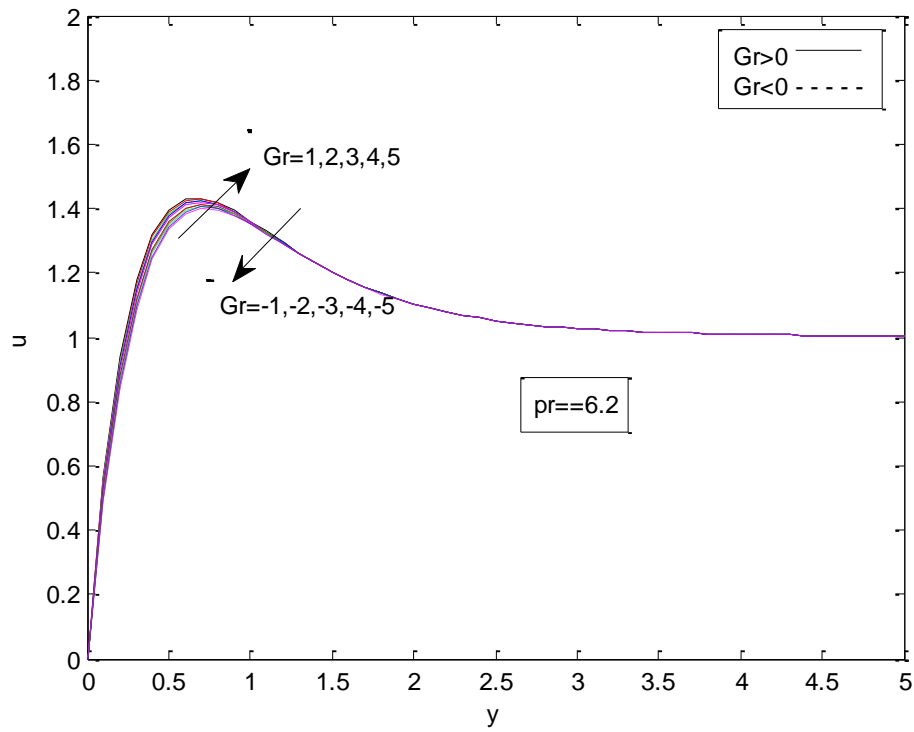
Figure 6. Velocity distribution for various values of Grash of number Gr for $\omega = 10$, $\omega t = \pi/2$, $\varepsilon = 0.5$, $N = 0.2$, $M = 10$, $G_c = 5$, $kr = 3$, pr=6.2, $Sc = 0.22$.
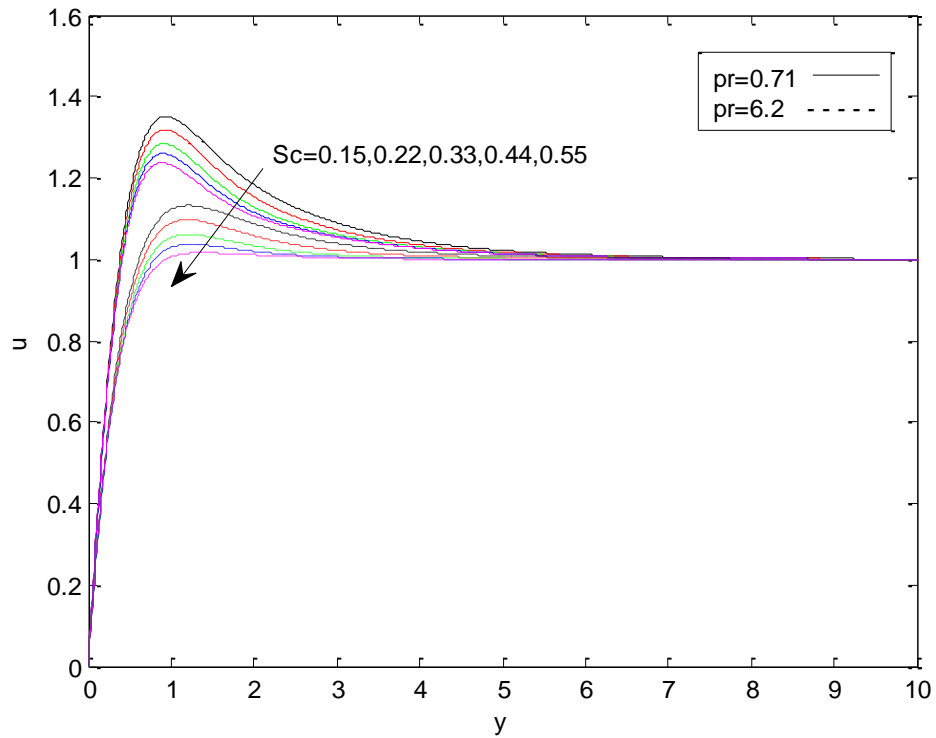
Figure 7. Velocity distribution for various values of Prandtl number Pr and the Schmidt number Sc for $\omega = 10$, $\omega t = \pi/2$, $\varepsilon = 0.5$, $N = 0.2$, $M=5$, $kr = 3$, $G_r = G_c = 2$,
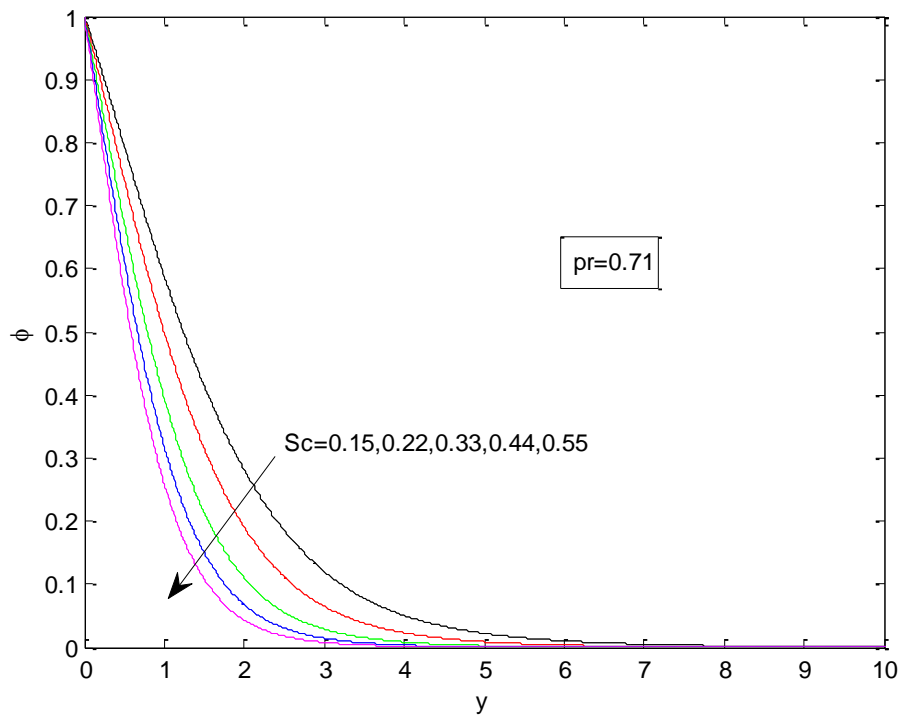
Figure 8. Concentration distribution for various values of the Schmidt number Sc for $\omega = 10$, $\omega t = \pi/2$, $\varepsilon = 0.5$, $N = 0.2$, $M=5$, $kr = 3$, $G_r = G_c = 2$
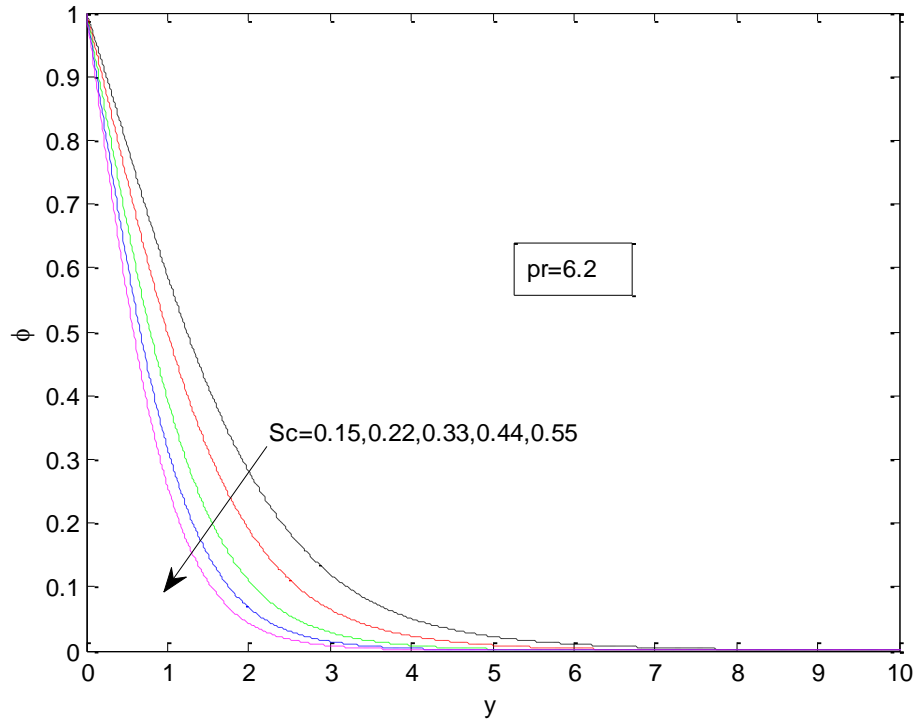
Figure 9. Concentration distribution for various values of the Schmidt number Sc for $\omega = 10$, $\omega t = \pi/2$, $\varepsilon = 0.5$, $N = 0.2$, $M=5$, $kr = 3$, $G_r = G_c = 3$, pr=6.2.

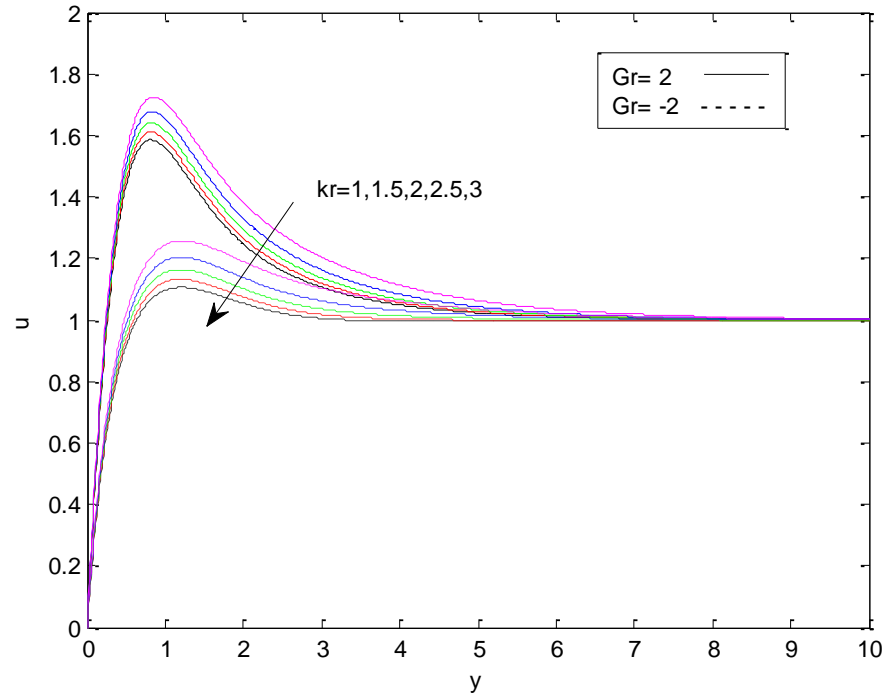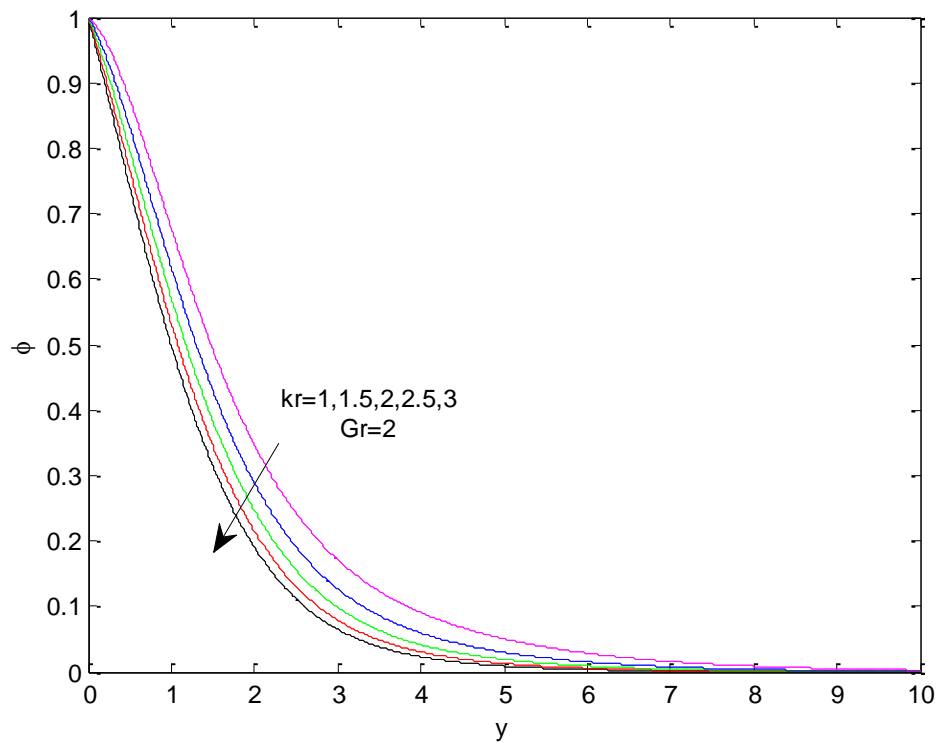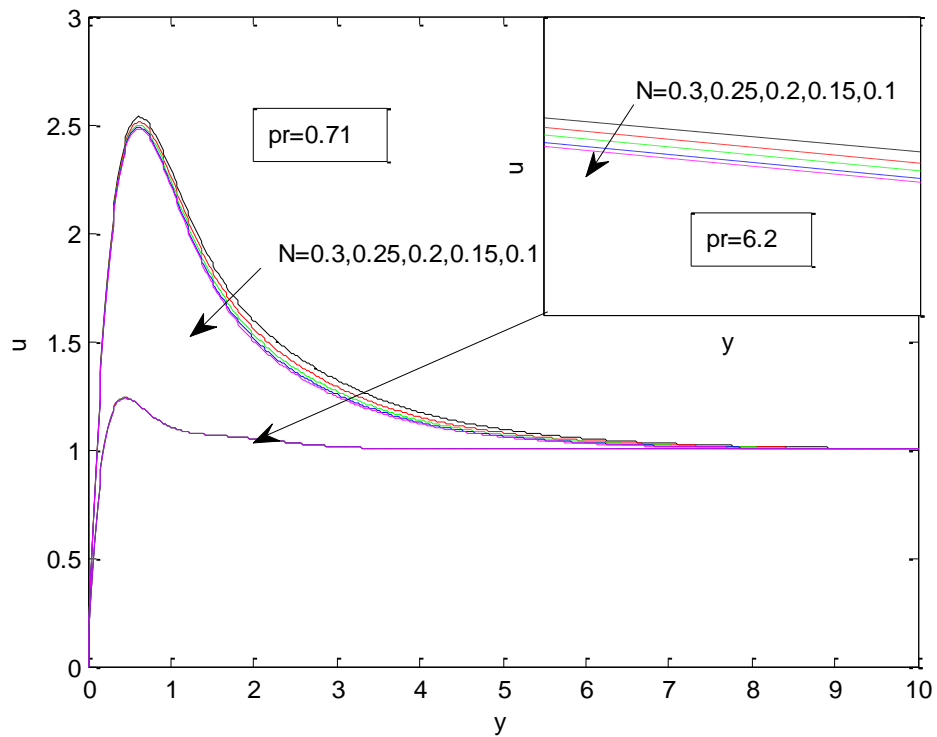**Figure 10.** Velocity distribution for various values of radiation parameter N for $\omega = 10$, $\omega t = \pi/2$, $\varepsilon = 0.5$, $Sc = 0.66$, $M=5$, $kr = 3$, $G_r = G_c = 5$.
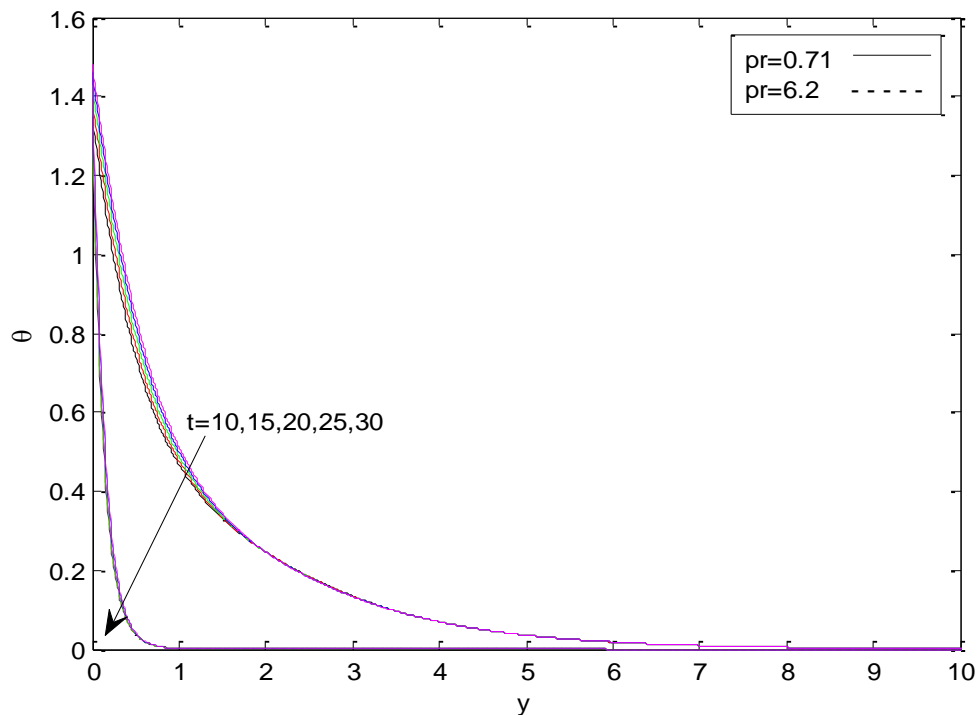
Figure 11. Temperature distribution for various values of Prandtl number Pr and the time t for $\omega = 5$, $\omega t = \pi/2$, $\varepsilon = 0.5$, $N = 0.2$, $M = 5$, $kr = 6$, $G_r = G_c = 5$, $Sc = 0.22$.

Table 1. Effects of variations of Grashof number, modified Grashof number, chemical reaction, Schmidt number, magnetic parameter, frequency of the fluid and radiation parameter on the coefficients of skin friction, heat transfer and mass transfer respectively for Pr=0.71, ωt=π/2 and ε=0.5.

Pr	Gr	Gc	kr	Sc	M	ω	N	C_f	$Nu\,\mathrm{Re}_x^{-1}$	$Sh\,\mathrm{Re}_x^{-1}$
	-2							0.9681985		
	0	-2	1	0.22	5	5	0.2	2.4504063	0.0104001	0.2278289
	2							3.9326142		
		0						6.0647835		
		2						8.1969528		
			2					8.0915512		0.4788251
			3					8.0292530		0.6521084
0.71				0.44				8.1965396		0.9988825
				0.66				8.6646388		1.2987692
					10			8.9164825		
					15			10.088027		
						10		9.5646458	-0.268168	0.9979852
						15		9.0859922	-0.481072	0.7734869
							0.3	9.1014427	-0.546189	
							0.4	9.1369066	-0.686658	

Table 2. Effects of variations of Grashof number, modified Grashof number, chemical reaction, Schmidt number, magnetic parameter, frequency of the fluid and radiation parameter on the coefficients of skin friction, heat transfer and mass transfer respectively for Pr=6.2, $\omega t=\pi/2$ and $\varepsilon=0.5$.

Pr	Gr	Gc	kr	Sc	M	w	N	C_f	$Nu\,\mathrm{Re}_x^{-1}$	$Sh\,\mathrm{Re}_x^{-1}$
	-2							1.9013410		
	0	-2	1	0.22	5	5	0.2	2.4504063	4.4633888	0.2578289
	2							2.9994716		
		0						5.1316409		
		2						7.2638104		
			2					7.1584088		0.4788251
			3					7.0961104		0.6521084
6.2				0.44				7.2633971		0.9988814
				0.66				7.7314962		1.2987690
					10			8.1253424		
					15			9.4666094		
						10		8.9347129	3.5775681	0.9979852
						15		8.4445792	2.9172851	0.7734869
							0.3	8.4469053	2.8608185	
							0.4	8.4502701	2.7802543	

Table 3. Effects of various values of time on the coefficients of skin friction, heat transfer and mass transfer respectively for $\omega = 5$, $\varepsilon = 0.5$, $N = 0.2$, $M= 10$, $G_r=G_c=2$, kr=3, Sc=0.22.

Pr	T	C_f	$Nu\,\mathrm{Re}_x^{-1}$	$Sh\,\mathrm{Re}_x^{-1}$
	0	14.6751855	1.5203172	1.4799403
	10	14.6269275	1.6628313	1.5335311
0.71	20	14.2328840	1.7356010	1.5448208
	30	13.5206649	1.7335276	1.5130185
	40	12.5401740	1.6567563	1.4403525
	50	11.3601122	1.5106664	1.3319143
	0	13.4775922	9.9940552	1.4799403
	10	13.4600055	10.304803	1.5335310
6.2	20	13.1268349	10.325115	1.5448208
	30	12.5014249	10.053568	1.5130185
	40	11.6275967	9.5091880	1.4403525
	50	10.5665778	8.7301189	1.3319143

the Nusselt number increases as Pr increases.

Finally, the effects of various values of t on the coefficients of skin friction, heat transfer and mass transfer across the boundary layer are presented in Table 3. It can be concluded that skin friction decreases as time increases. Heat and mass transfer increase with time at values 0, 10, and 20, while decreasing at values 20, 30, 40, and 50.

Conclusion

An analytical solution for two-dimensional oscillatory flow on unsteady mixed convection of an incompressible viscous fluid, through a porous medium bounded by an infinite vertical plate in the presence of chemical reaction and thermal radiation are presented. The governing boundary layer equations for the velocity, temperature, and concentration fields were solved using the method of small perturbation approximation. Numerical evaluation of the analytical solutions was performed and the results were presented in graphical and tabular form. This was done to illustrate the influence of the various parameters involved in the problem on the solutions. Two cases can be considered air ($P_r = 0.71$) and water ($P_r = 6.2$). It can be concluded that the velocity in the case of cooling and heating decreases near the boundary with an increase in the chemical reaction. Also, increasing the chemical reaction is to decrease the concentration profile throughout the boundary layer. Also, it was found that for two values of Prandtl number, under study, the concentration distribution decreases as the Schmidit number increases. Moreover, the Nusselt number decreases as the Prandtl number increases. It is interesting to note that the rate of heat mass transfer increase with increasing time for both air and water when $t \leq 20$, while the reverse behavior is observed when $t \geq 20$.

CONFLICT OF INTERESTS

The authors have not declared any conflict of interests.

REFERENCES

Abdelkader K, Lounes O (2007). Heat transfer enhancement in oscillatory flow in channel with periodically upper and lower walls mounted obstacles. Int. J. Heat Fluid Flow. 28:1003-1012.

Anjali Devi SP, Kandasamy R (2002). Effects of chemical reaction, heat and mass transfer on non-linear MHD laminar boundary layer flow over a wedge with suction and injection. Int. Comm. Heat Mass Transf. 29:707-716.

Bakr AA (2011). Effects of chemical reaction on MHD free convection and mass transfer flow of a micropolar fluid with oscillatory plate velocity and constant heat source in a rotating frame of reference. Comm. Non. Sci. Numer. Simulat.16:698-710.

Chambre PL, Young JD (1958). On the diffusion of chemically reactive species in a laminar boundary layer flow. Phys. Fluids 1:48-54.

Chamkha A (2003). MHD flow of uniformly stretched vertical permeable surface in the presence of heat generation absorption and a chemical reaction. Int. Comm. Heat Mass Transf. 30:413-422.

Cooper WL, Nee VW, Yang KT (1993). Fluid mechanics of oscillatory and modulated flows and associated applications in heat and mass transfer - a review. J. Energ. Heat Mass Transf. 15:1-19.

Cussler EL (1998). Diffusion Mass transfer in fluid Systems. 2nd Ed, Cambridge University Press. Cambridge.

Das UN, Deka RA, Soundalgekar VM (1994). Effect of mass transfer on flow past an impulsively started infinite vertical plate with constant heat flux and chemical reaction. Forsch. Ingen. 60:284-287.

El-Hakiem MA (2000). MHD oscillatory flow on free convection-radiation through a porous medium with constant suction velocity. J. Magn. Magn. Mater. 220:271-276.

Fusegi T (1997). Numerical study of convective heat transfer from periodic open cavities in a channel with oscillatory through flow. Int. J. Heat Fluid flow. 18:376-383.

Gholizadeh A (1990). MHD oscillatory flow past a vertical porous plate through porous medium in the presence of thermal and mass diffusion with constant heat source. Astr. Space Sci. 174:303- 310.

Gomaa H, Al Taweel AM (2005). Effect of oscillatory motion on heat transfer at vertical flat surfaces. Int. J. Heat Mass Transf. 48:1494-1504.

Hakeem AK, Sathiyanathan K (2009). An analytic solution of an oscillatory flow through a porous medium with radiation effect. Non. Analy. Hybrid Systems 3:288-295.

Kandasamy R, Periasamy K, Sivagnana Prabhu KK (2005). Chemical reaction, heat and mass transfer on MHD flow over a vertical stretching surface with heat source and thermal stratification effects. Int. J. Heat Mass Transf. 48:45-57.

Makinde OD (1994). Unsteady incompressible flow in a porous channel. Proc. Rom. Appl. Indust. Math. Oradea. pp. 47-58.

Makinde OD, Aziz A (2010). MHD mixed convection from a vertica plate embedded in a porous medium with a convective boundary condition. Int. J. Therm. Sci. 49:1813-1820.

Makinde OD, Mhone PY (2005). Heat transfer to MHD oscillatory flow in a channel filled with porous medium. Rom. J. Phys. 50:931-938.

Mehmood A, Ali A (2007). The effect of slip condition on unsteady MHD oscillatory flow of a viscous fluid in a planer channel. Rom. J. Phys. 52:85-91.

Muthucumaraswamy R (2001). First order chemical reaction on flow past an impulsively started vertical plate with uniform heat and mass flux. Act. Mech. 147:45-57.

Muthucumaraswamy R (2002). Effect of a chemical reaction on a moving isothermal vertical surface with suction. Act. Mech. 155:65-70.

Pal D, Talukdar B (2010). Perturbation analysis of unsteady magnetohydrodynamic convective heat and mass transfer in a boundary layer slip flow past a vertical permeable plate with thermal radiation and chemical reaction. Comm. Non. Sci. Numer. Simulat. 15:1813–1830.

Prakash J, Sivaraj R, Kumar B (2011). Influence of chemical reaction on unsteady MHD mixed convective flow over a moving vertical porous plate. Int. J. fluid Mechan. 3(1):1-14.

Rabi N, Gouranga C, Arpita M (2013). Chemical reaction effect on MHD Oscillatory flow through a porous medium bounded by two vertical porous plates with heat source and soret effect. J. Appl. Analy. Comput. 3(4):307-321.

Saxena SS, Dhiresh KP, Sandeep K (2014). MHD free convective oscillatory Rivlin-Ericksen fluid flow past a porous plate embedded in a porous medium in the presence of heat source with chemical reaction. Der Chem. Sinic. 5(4):30-45.

Sivaraj R, Kumar BR (2011). Chemically Reacting Unsteady MHD Oscillatory Slip Flow in a Planer Channel with Varying Concentration. Int. J. Math. Scientific Comput. 1(1):35-42.

Srinivas S, Muthuraj R (2010). Effects of thermal radiation and space porosity on MHD mixed convection flow in a vertical channel using homotopy analysis method. Comm. Non. Sci. Numer. Simulat. 15:2098-2108.

Vajravelu K (1986). Hydrodynamic flow and heat transfer over Continuous, Moving Porous, Flat Surface. Acta Mech. 64:179-185.

Full Length Research Paper

Simulation of the impact of climate change on peanut yield in Senegal

Alioune Badara Sarr and Moctar Camara*

Laboratoire d'Océanographie, des Sciences de l'Environnement et du Climat (LOSEC), UFR Sciences et Technologies, Université A. SECK de Ziguinchor, Sénégal.

This paper treats the impacts of climate change on peanut yield in Ziguinchor (Southwest of Senegal) during the near future (2021 to 2050) and the far future (2071 to 2100). The Decision Support System for Agrotechnology Transfer (DSSAT) crop model was run using daily weather data (maximum and minimum surface temperature, rainfall and solar radiation) of four (4) regional climate models (RCMs) of the Coordinated Regional Climate Downscaling Experiment (CORDEX). Two climate change scenarios (RCP4.5 and RCP8.5) are used to assess the climate change impact on peanut yield. First of all, the DSSAT crop model is calibrated and validated for peanut using relevant observed data: peanut yield and meteorological data. Compared to the reference period (1976 to 2005), the RCMs exhibit some disparities in the projected rainfall during the near and the far future. The ensemble mean of the models (Ens/RCMs) predict a strong decrease of rainfall under the RCP4.5 scenario and a slight decrease under the RCP8.5 scenario during both periods. A gradual increase in mean temperature is predicted by all models. However, this increase is stronger for the RCP8.5 scenario. Analysis of the yield change during the near future shows a decrease for all RCMs except RACMO22T model under the two considered scenarios. During the far future, all RCMs predict a decrease of the peanut yield. Moreover, this decrease is stronger for the RCP8.5 scenario. These results indicated that the peanut crop could be negatively affected by the climate change and adaptation strategies are needed to protect this sector.

Key words: Climate change, Regional Climate Models, Coordinated Regional Climate Downscaling Experiment (CORDEX), Decision Support System for Agrotechnology Transfer (DSSAT), peanut.

INTRODUCTION

Senegal, like other West African countries is very vulnerable to climate change. According to the Intergovernmental Panel on Climate Change (IPCC, 2013), these climate changes are most probably due to the anthropic greenhouse gas emissions which carbon dioxide is the most important. In the semi-arid countries like Senegal, this translates into an increase in temperature, a reduction of the summer rainfall amount and an increase in certain extreme events such as the floods and the droughts (Giorgi et al., 2014; Diallo et al., 2016;

Sarr and Camara, 2017). Agriculture plays a significant role in the livelihood and economy growth of most African people (Kotir, 2010). The Senegalese economy depends heavily on agriculture and more particularly on the peanut cultivation which is the major crop grown in this country (Kouadio, 2007; Noba et al., 2014). Agriculture constitutes approximately 46% of the country's total land area and supports 70% of the rural population (Colen et al., 2013; FAO, 2014). However, certain human activities such as agriculture are expected to be vulnerable to climate change (Salack et al., 2015). Moreover, in the semi-arid regions of West Africa like the Sahel, the adaptation capacity is very low (Boko et al., 2007). Then, the climate change can aggravate the problem of food security in this region and particularly in Senegal. According to Food and Agriculture Organization of the United Nations (FAO, 2016), some eleven (11) million people still suffer from severe food insecurity in the Sahel. In Senegal, for example 47% of the population lives below the national poverty line according to the Climate-Smart Agriculture (CSA, 2016). To remedy this, it is necessary to develop strategies to build a resilient agriculture. This has often been biased by the bad interpretation of seasonal forecasts by farmers and the lack of reliable climate projections so that the long-term planning is not clearly determined. To address this question, we will make agro-meteorological forecasts to study the impact of climate change on agriculture. This requires coupling crop model with climate models (Rezzoug and Gabrielle, 2015; Waha et al., 2015). The crop model plays significant role in climate change impacts assessment on agriculture. As crop models simulate at scales closer to the farm, forcing it with high resolution regional climate models (RCMs) (~10-50 km) outputs seems to be more appropriate. This will produce relevant information for agricultural decision makers.

This paper aims at simulating the peanut yield response to future climate change in Ziguinchor (Senegal) using the DSSAT crop model forced by the outputs of four (4) RCMs of CORDEX program. CORDEX is an international program implemented by several research centers which aim is to produce reliable climate change scenarios for impact studies (Giorgi et al., 2009). The CORDEX RCMs outputs have been thoroughly validated over West Africa (Nikulin et al., 2012; Akinsanola and Ogunjobi, 2017; Klutse et al., 2015). The climate change projections data are obtained by forcing CORDEX regional climate models by the Coupled Model Inter Comparison Project phase 5 (CMIP5) global climate models from the period 1951 to 2100 (Giorgi et al., 2009; Nikulin et al., 2012).

DATA AND METHODS

Description of the study area

The study area is situated in the Diabir district of the city of

Ziguinchor (Figure 1), particularly in the National Center of Training of the Technicians in Agriculture and in Rural Genius of Ziguinchor (16°17'12''W , 12°33'40'' N, 10 m above the mean sea level). The city of Ziguinchor is located in the Southwestern part of Senegal (Figure 1). Its agriculture is essentially rain-fed. The minimum and maximum daily air temperatures in this city range between 22.8 and 34.0°C, respectively, while the mean annual rainfall is about 1200 mm. More than 90% of rainfall is recorded between June and September. Summary of some climate relevant parameters during the growing season is shown in Table 1. The soil texture of the experimental farm is dominantly sandy-loam. A soil sampling was carried out and the results are shown in Table 2.

Crop model description

The Decision Support System for Agrotechnology Transfer (DSSAT) crop model is used in this study. It is a set of computer programs for simulating agricultural crop growth that was designed and implemented by an international network of scientists, cooperating in the International Benchmark Sites Network for Agrotechnology Transfer project (IBSNAT) (1993) and Jones et al. (1998). The DSSAT includes the effects of crop phenotype, soil profiles, weather data and management options into a crop model. This model takes into account more than 20 crop varieties. It can simulate peanut growth and development at daily time step from sowing to maturity and finally predict the crop yield. The minimum daily weather data required to run the DSSAT model includes daily precipitation, daily maximum and minimum temperatures and daily solar radiation. The DSSAT model has been extensively used worldwide to simulate the impact of climate change on crops (Rezzoug and Gabrielle, 2015; Waha et al., 2015; Salack et al., 2015). In this study, the crop model is used to estimate the impact of climate change on the peanut variety Virginia 897 during the near and the far future.

Crop management data

All the crop management data required by the model was obtained from the experimental field of the National Center of Training of the Technicians in Agriculture and in Rural Genius of Ziguinchor during the year 2016. The planting date was set to the day of year (DOY) 201, that is, 19th July, 2016 and the relative maturity of peanut is about 90 days. The spacing between the lines and the poquets were respectively 60 cm and 16 cm. The plot size is 20 × 25 m. The planting depth was 5 cm and population density was 3 plants per m². An initial nitrogen fertilizer of 150 kg/ha was applied.

Climate change scenarios and yield prediction

The DSSAT crop model was run using daily weather data (maximum and minimum air temperature, solar radiation and precipitation) generated from 4 RCMs of CORDEX program. They are CCLM4, RCA4, RACMO22T and HIRHAM5 models. CORDEX RCMs outputs can be downloaded from the following link: https://www.cordex.org/output.html. The horizontal resolution of these models is 0.44° (approx. 50 km). The models institutions, the global climate model forcing and the references are shown in Table 3. The climate change projections are obtained by forcing the regional climate model by the outputs of global climate model (GCM) under greenhouse gases emission scenarios RCP4.5 and RCP8.5. The RCP4.5 (or medium scenario) and RCP8.5 (or pessimistic scenario) scenarios correspond to emissions of 4.5 and 8.5 W/m² of greenhouse gases, respectively. These RCPs forcing scenarios have been described in details by Moss et al. (2010). The considered periods for this study are the reference period (1976 to
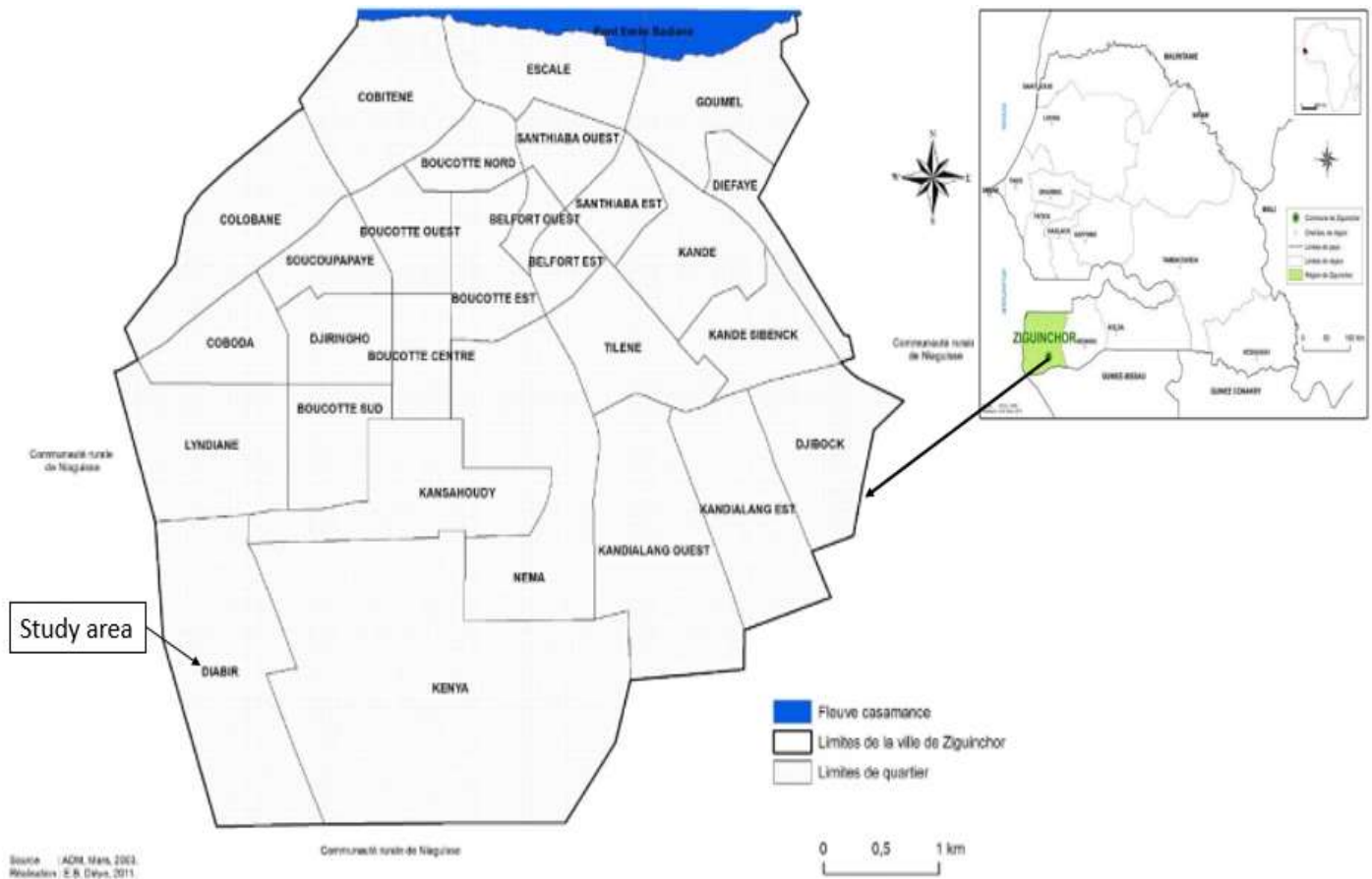
Figure 1. Study area.
Source: Mbaye (2016).

Table 1. Mean monthly weather parameter during the year 2016.

Month	Minimum temperature (°C)	Maximum temperature (°C)	Rainfall (mm)
Jan	19.7	32.8	0
Feb	19.3	35.2	0
Mar	20.4	36.5	0
Apr	20.6	35.5	0
May	21.3	34.2	5.59
Jun	23.6	32.7	57.7
Jul	24.1	30.7	356
Aug	24.2	31.0	407
Sep	23.9	31.6	430
Oct	24.6	33.1	38.1
Nov	23.3	33.1	0
Dec	21.1	31.9	0

2005), the near future (2021 to 2050) and the far future (2071 to 2100). The climate in Senegal is Sahelian, that is, characterized by one rainy season (from June to September) called the summer season characterized by rain-fed agriculture. This work focuses on the summer period.

For the impact assessment, a statistical downscaling method (delta change approach) is applied in this study. In this method, the daily variability is assumed to have the same magnitude during the

Table 2. Soil characteristics of the study area.

Soil depth (cm)	pH in water	N (ppm)	P (ppm)	Soil organic carbon (%)	Bulk density (g.cm^{-3})
0-5	6.4	5.52	6.7	3.8	1.3
5-20	6.0	1.46	0.21	2.8	1.1

Table 3. Description of the regional climate models.

Name	GCM forcing	Institution	References
CCLM4	CNRM-CM5	CLM-community	Baldauf et al. (2011)
RACMO22T	EC-EARTH	KNMI, The Netherlands	Van Meijgaard et al. (2008)
RCA4	CNRM-CM5	SMHI, Sweden	Samuelsson et al. (2011)
HIRHAM5	EC-EARTH	DMI, Denmark	Christensen et al. (2006)

future and the reference periods (Hawkins et al., 2012; M'Po et al., 2016). The delta change approach is defined by the following equations:

$$P_{corr} = P^* \frac{\overline{P_{obs}}}{\overline{P_{ref,RCM}}} \tag{1}$$

$$Srad_{corr} = Srad^* \frac{\overline{Srad_{obs}}}{\overline{Srad_{ref,RCM}}} \tag{2}$$

$$T_{corr} = T^* + (\overline{T_{obs}} - \overline{T_{ref,RCM}}) \tag{3}$$

where P_{corr}, $Srad_{corr}$ and T_{corr} are the corrected daily precipitation, solar radiation and temperature. P^*, $Srad^*$ and T^* are the corresponding uncorrected daily precipitation, solar radiation and temperature. $\overline{P_{obs}}$, $\overline{Srad_{obs}}$, $\overline{T_{obs}}$, $\overline{P_{ref,RCM}}$, $\overline{Srad_{ref,RCM}}$, $\overline{T_{ref,RCM}}$ are the mean values of observed and simulated daily precipitation, solar radiation and temperature during the reference period.

RESULTS

Model calibration and performance

The DSSAT model was calibrated for peanut using the experimental data provided by the national center of training of the technicians in agriculture and in rural genius (soil characteristics, peanut yield, etc) and the observed daily weather data (minimal and maximal temperature, solar radiation and precipitation) of the Assane Seck University of Ziguinchor during the year 2016 which is located in the same area than the experimental farm. The process of calibration aims at obtaining reasonable estimates of model genetic coefficients by comparing simulated data with those

observed. The genetic coefficient of the cultivars (Virginia 897) calibrated in DSSAT is presented in Table 4. Using this calibrated genetic coefficient, results show that the simulated days to anthesis, days to physiological maturity and grain yield are very close to those observed (Table 5). This step is a prerequisite for the crop model to estimate reasonably the possible impact of climate change on peanut yield.

Climate change scenarios during the near future (2021-2050)

The summer rainfall change during the near future (2021 to 2050) with respect to the historical period is shown in Figure 2. These rainfall projections show contrasted results with increases and decreases in rainfall during the monsoon season (JJAS). The simulated rainfall under the two RCPs scenarios is also highly variable. The RACMO22T model shows the strongest rainfall increase with highest simulated values for the RCP8.5 scenario (up to 7%). The CCLM4 and RCA4 models show a decrease under the RCP4.5 scenario and a weak increase under the RCP8.5 scenario. An increase is diagnosed for the RACMO22T model with values reaching 3% under RCP4.5 and 8% under RCP8.5 scenario. The HIRHAM5 model shows the strongest rainfall decrease for both scenarios (up to 12% for the RCP4.5 scenario and 17% for the RCP8.5 scenario). The ensemble mean of the models (arithmetic mean of the regional climate models) shows a decrease of about 6% under the RCP4.5 scenario and no significant changes under RCP8.5 scenario.

Concerning the seasonal change in temperature during the near future (Figure 3), the results revealed that temperature will rise in the near future for all RCMs. This increase in temperature could exceed 1°C with stronger values for the RCP8.5 scenario. The maximum temperature rise is recorded with the HIRHAM5 model

Table 4. Genetic coefficient of peanut cultivars calibrated in DSSAT (Virginia 897).

Coefficient	Definition	Value
CSDL	Critical short day length below which reproductive development progresses with no day length effect (h)	11.84
PP-SEN	Slope of the relative response of development to photoperiod with time Phenology (h^{-1})	0.00
EM-FL	Time between plant emergence and flower appearance (R1) (photothermal days)	21.0
FL-SH	Time between first flower and first peg (R2) (photothermal days)	8.0
FL-SD	Time between first flower and first seed (R5) (photothermal days)	20.0
SD-PM	Time between first seed (R5) and physiological maturity (R7) (photothermal days)	78.00
FL-LF	Time between first flower (R1) and end of leaf expansion (photothermal days)	85.00
SFDUR	Seed filling duration for pod cohort at standard growth conditions (photothermal days)	38
PODUR	Time required to reach final pod load under optimal conditions Growth (photothermal days)	30
LFMAX	Maximum leaf photosynthesic rate at 30°C, 350 vpm CO_2, and high light (mg $CO_2/m^{-2}s^{-1}$)	1.30
SLAVR	Specific leaf area under standard growth conditions (cm^2g^{-1})	275
SIZLF	Maximum size of full leaf (three leaflets) (cm^2)	20
XFRT	Maximum fraction of daily growth that is partitioned to seed + shell	0.76
WTPSD	Maximum weight per seed (g)	0.96
SDPDV	Average seed per pod under standard growing conditions (Numbers per pod)	1.65

Table 5. Observed and simulated for peanut yield.

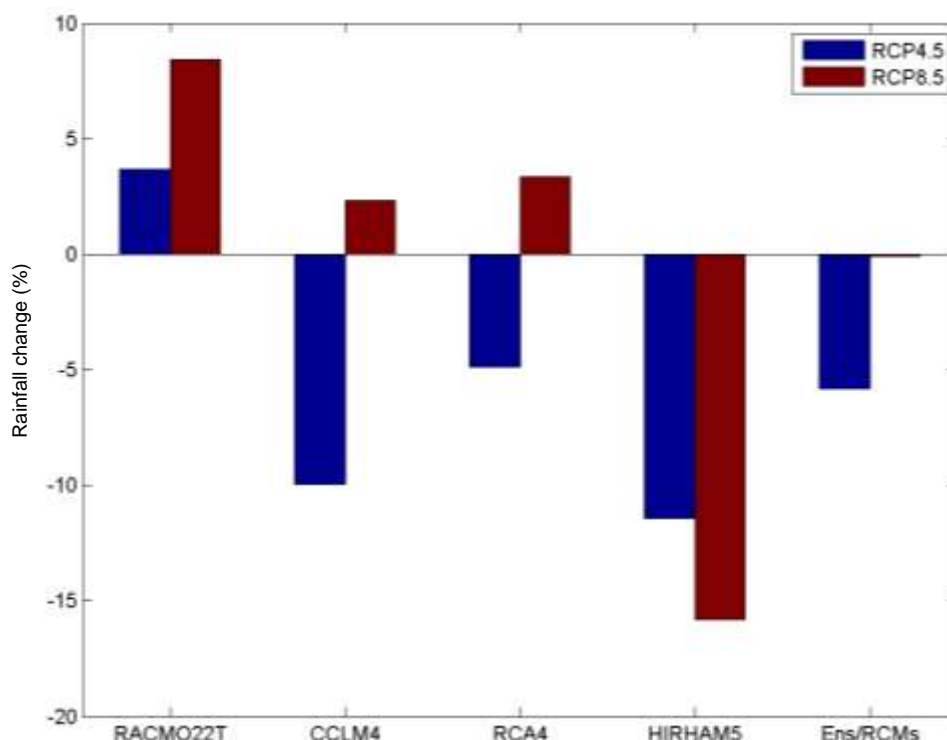| Variable	Observed	Simulated	Difference
Flowering date (DOY)	221	217	-4
Maturity date (DOY)	298	301	3
Grain yield (kg/ha)	1200	1198	-2

Figure 2. Projected changes of JJAS rainfall (expressed in %) during the near future (2021 to 2050) with respect to the reference period for RACMO22T, CCLM4, RCA4, HIRHAM5 models and their ensemble mean (Ens/RCMs) under the RCP4.5 and RCP8.5 scenarios.

Figure 3. Projected changes of JJAS temperature (expressed in °C) during the near future (2021 to 2050) with respect to the reference period for RACMO22T, CCLM4, RCA4, HIRHAM5 models and their ensemble mean (Ens/RCMs) under the RCP4.5 and RCP8.5 scenarios.

under the RCP8.5 scenario and the minimum with the RCA4 model under the RCP4.5 scenario. This trend of increased temperature is consistent with Kouakou et al. (2014) findings who indicated the same range of increased temperature for the horizon 2031 to 2040 in the Sahel region.

Climate change scenarios during the far future (2071-2100)

Figure 4 shows the seasonal rainfall change during the far future (2071 to 2100) with respect to the reference period for the RCMs and their ensemble mean. Rainfall changes in the far future present some uncertainties. The RACMO22T model shows a strong increase of rainfall for both scenarios especially under the RCP8.5 scenario (up to 15%). This rainfall strengthening will be stronger by 2100 than in the near future. An increase in rainfall is also simulated in the case of the RCA4 model for both scenarios but it is lower when compared to the RACMO22T. The CCLM4 model as well as the ensemble mean of the models show a strong rainfall decrease under the RCP4.5 scenario (about 22% for CCLM4 and 7% for the ensemble mean of the model) and a slight decrease under the RCP8.5 scenario. The HIRHAM5

model exhibits a strong decrease of rainfall for both scenarios (about 20 and 23% for RCP4.5 and RCP8.5 scenarios respectively) and this decrease is stronger in the far future.

Figure 5 shows the mean summer temperature change during the far future (2071 to 2100) for the RCMs and their ensemble mean. In this period, a significant warming is predicted which is in line with some works (Kouakou et al., 2014; Sylla et al., 2016) who indicated that temperature will continue to rise over all West Africa and especially in the Sahel region whatever the considered scenarios types. This possible increase of the surface temperature is associated with an increase of water demand on many sector particularly the agriculture. The range of change in temperature during the far future with respect to the reference period (1976 to 2005) varies from a regional climate model to another one. The increase is about 1.8 to 2°C under RCP4.5 scenario and 3.3 to 3.7°C under RCP8.5 scenario in the far future. These latest results (obtained with RCP8.5 scenario) are consistent with those in IPCC report (2013) who diagnosed a temperature rise ranging between 3 and 3.5°C by 2100 in the Sahel region. The strongest temperature rise is simulated by the CCLM4 model under the RCP8.5 scenario. The RCA4 model shows the weakest increase for both scenarios. It should also be

Figure 4. Projected changes of JJAS rainfall (expressed in %) during the far future (2071 to 2100) with respect to the reference period for RACMO22T, CCLM4, RCA4, HIRHAM5 models and their ensemble mean (Ens/RCMs) under the RCP4.5 and RCP8.5 scenarios.
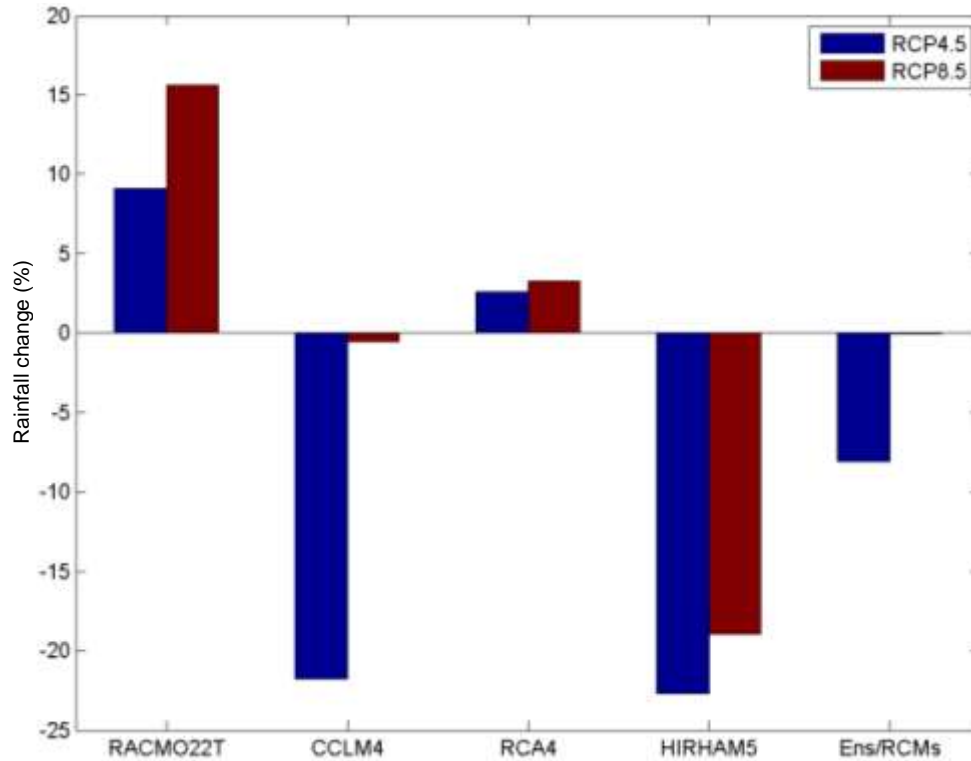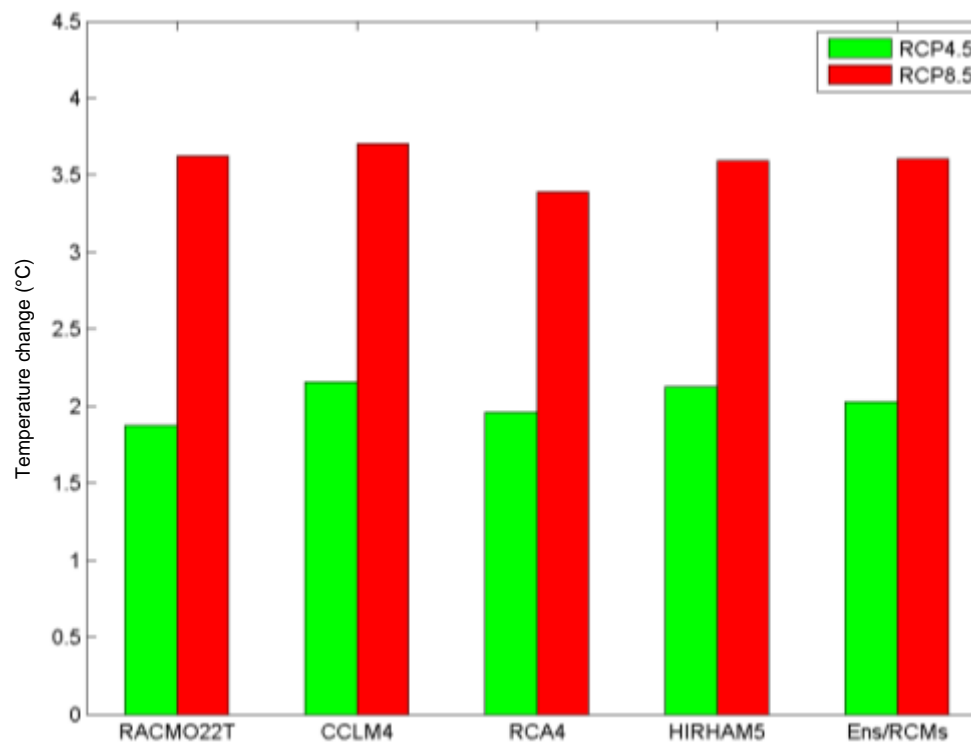

Figure 5. Projected changes of JJAS temperature (expressed in °C) during the far future (2071 to 2100) with respect to the reference period for RACMO22T, CCLM4, RCA4, HIRHAM5 models and their ensemble mean (Ens/RCMs) under the RCP4.5 and RCP8.5 scenarios.
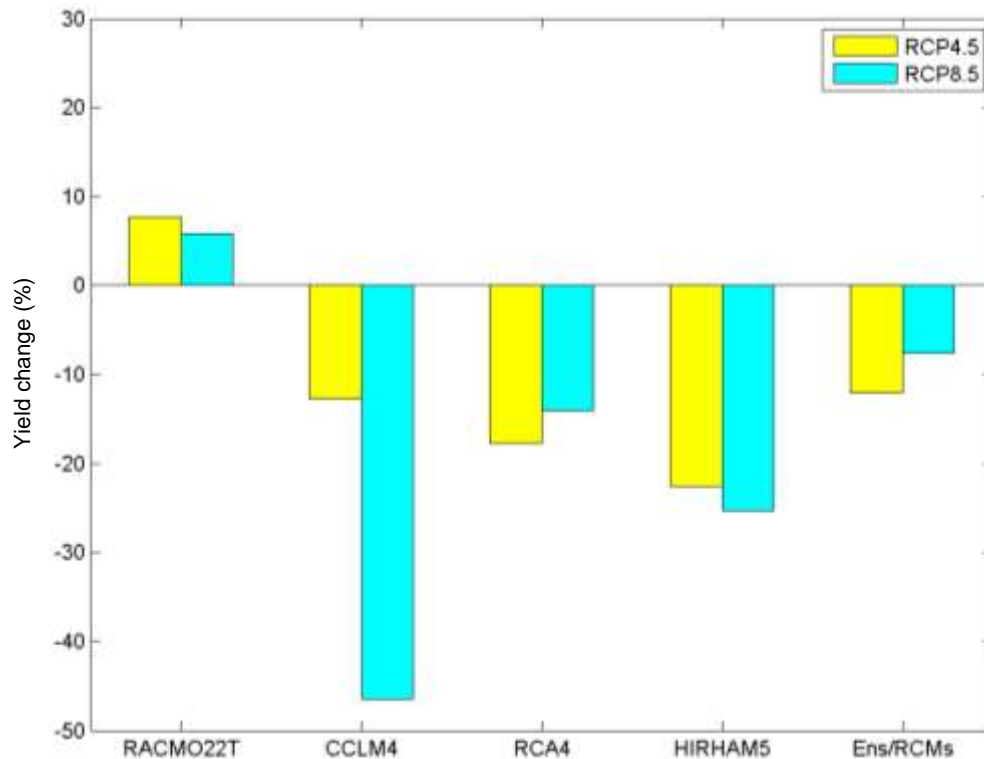
Figure 6. Percent yield change during the near future (2021 to 2050) with respect to reference period for RACMO22T, CCLM4, RCA4, HIRHAM5 models and their ensemble mean (Ens/RCMs) under the RCP4.5 and RCP8.5 scenarios.

pointed out that the surface temperature is stronger in the far future when compared to the near future for all models. The stronger warming predicted by the RCMs under the RCP8.5 scenario compared to the RCP4.5 can be explained by the fact that the rise of temperature is induced by the increase of greenhouse gases concentration (IPCC, 2013). Compared to near future, a gradual increase in temperature is noted. Changes in temperature and rainfall could affect crop production (Salack et al., 2015; Potop et al., 2014). In the last part of this results discussion, we investigate the possible climate change impact on peanut cultivation during the near and the far future.

Projections of peanut yield during the near future

Figure 6 shows the projected change in peanut yield during the near future simulated by DSSAT crop model forced by the RCMs outputs. Results show many disparities in the predicted yield but these variations are not very strong. A decline in peanut yields is diagnosed for all models except the RACMO22T. The RACMO22T model under the two scenarios shows a slight increase of peanut yields (about 7 and 5% for RCP4.5 and RCP8.5 scenarios, respectively) during the near future. These

results could be partly explained by the predicted increase in rainfall simulated by this model during the near future. However, other RCMs and the ensemble mean of models show a decrease of peanut yields. The strongest (lowest) decrease is shown by the CCLM4 model under the RCP8.5 (RCP4.5) scenario. The ensemble mean of all models exhibits a weak peanut yield decrease for both scenarios. The projected peanut yield decrease obtained with the CCLM4 and RAC4 models under the RCP8.5 scenario is not consistent with the rainfall increase simulated under the same scenario. However, this decline in peanut yield seems to be consistent with the strong increase of surface temperature simulated under this scenario because strong temperature increases are known to affect negatively the agricultural production.

Projections of peanut yield during the far future

Analysis of the change in the peanut yield during the far future is shown in Figure 7. All RCMs predict a strong decline of the peanut yield. This decrease is also stronger for the RCP8.5 scenario when considering all RCMs. HIRHAM5 under the RCP8.5 scenario exhibits the strongest decline with values reaching 45% followed by
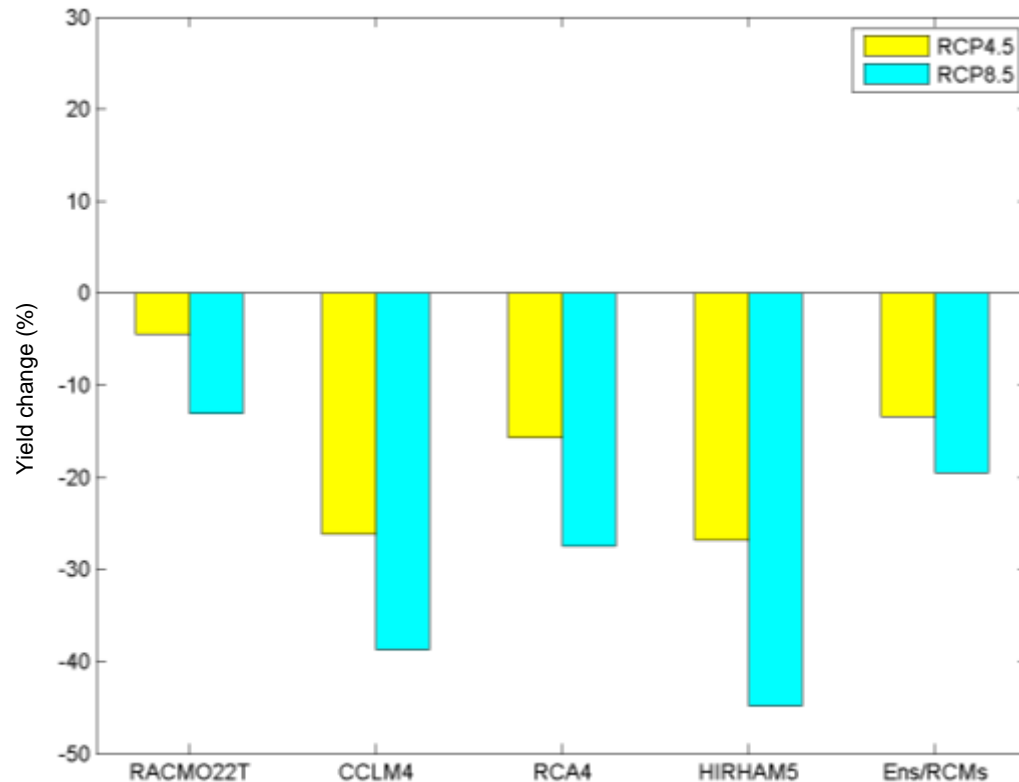
Figure 7. Percent yield change during the far future (2071 to 2100) with respect to reference period for RACMO22T, CCLM4, RCA4, HIRHAM5 models and their ensemble mean (Ens/RCMs) under the RCP4.5 and RCP8.5 scenarios.

the CCLM4 and the RCA4 models under the same scenario (about 38%). The lowest decrease is shown by the RACMO22T model. This decrease may be due to the fact that high greenhouse gases emissions may translate into a strong increase of the surface temperature which could inhibit the flowering (Jones et al., 1984; Araya et al., 2015). Thus, the decrease in peanut yield could be partly attributed to the strong increase of temperature predicted by most of the RCMs during the far future. It is difficult to determine exactly the role of temperature and rainfall changes in yield changes. According to Msongaleli et al. (2014), yield changes in arid zones appear to be mainly driven by rainfall changes. In Senegal for example, agriculture is essentially rain-fed (Salack et al., 2011). Thus, in case of water deficit, the production can be reduced due to the water insufficiency necessary to irrigate naturally plants. Nevertheless, in some cases, temperature changes can also affect the peanut growth. Indeed, increased temperature may have some impact on water demand of the crop as pointed out by Araya et al. (2015). Some authors (Abrol and Ingram, 1996; Salack et al., 2015) also stated that the strong rise in temperature can also affect the grain weight and the duration of grain growth.

To summarize, this study shows that in most cases climate change would affect negatively the peanut yield in the study area. Moreover, the impact of temperature and rainfall changes on peanut yield could not be separated.

Conclusion

Climate change is expected to highly affect the rain-fed agriculture in the Sahel region, particularly in Senegal. To analyze the peanut yield response to the future climate change, the DSSAT crop model was run using the outputs of four (4) CORDEX RCMs (minimum and maximum temperature, rainfall and solar radiation) under two climate change scenarios: RCP4.5 and RCP8.5. The analysis of the future precipitation and temperature change shows that there are many disparities in the projected rainfall simulated by regional climate models. This disagreement may be due to the internal variability of models (Paeth et al., 2011; Mariotti et al., 2011). The ensemble mean of the models shows a decrease which is stronger for the RCP4.5 scenario during the two future periods. Concerning the change in the surface temperature, RCMs show the same trend characterized by a gradual increase in the future especially under the RCP8.5 scenario. To be able to better analyze the future impact of climate change in peanut yield, we first calibrated and validated the DSSAT the crop model for

peanut using observed daily weather data and peanut yield. The results showed that the RCMs exhibit a decrease in peanut yield whatever the considered scenario, except the RACMO22T model which shows an increase for both scenarios during the near future. However, all RCMs agree on a decrease of peanut yield during the far future. Higher peanut yield reduction are observed for the RCP8.5 scenario. Many studies (Klutse et al., 2015; Nikulin et al., 2012; Diallo et al., 2012) show that the ensemble mean of models outperform individual RCMs suggesting that the RCA4 model may be more appropriate for use in this study area because its peanut yield change is closer to that of the ensemble mean of the models. This study also shows that it is difficult to separate the relative contribution of the surface temperature and rainfall in agriculture yields. Finally, the results of this study highlight the fact that it is necessary for the decision makers to set up appropriate adaptation measures to minimize the effects of climate change on agriculture especially on peanut culture. The necessary adaptation measures may include changes on the sowing date and the genotype selection.

CONFLICT OF INTERESTS

The authors have not declared any conflict of interests.

ACKNOWLEDGEMENTS

REFERENCES

Abrol YP, Ingram KT (1996). Effects of higher day and night temperatures on growth and yields of some crop plants. In: Bazzaz F, Sombroek W (eds) Global climate change and agricultural production. Direct and indirect effects of changing hydrological, pedological and plant physiological processes. Wiley, Chichester, pp. 124-140.

Akinsanola AA, Ogunjobi KO (2017). Evaluation of present-day rainfall simulations over West Africa in CORDEX regional climate models. Environ. Earth Sci. 76(10):366.

Araya A, Girma A, Getachew F (2015). Exploring Impacts of Climate Change on Maize Yield in Two Contrasting Agro-Ecologies of Ethiopia. Asian J. Appl. Sci. Eng. 4:27-37.

Baldauf M, Seifert A, Förstner J, Majewski D, Raschendorfer M, Reinhardt T (2011). Operational convective-scale numerical weather prediction with the COSMO model: description and sensitives. Mon. Wea. Rev. doi:10.1175/MWR.-D-10-05013.1.

Boko M, Niang I, Nyong A, Vogel C, Githeko A, Medany M, Osman-Elasha B, Tabo R, Yanda P (2007). Africa. Climate Change 2007: Impacts, Adaptation and Vulnerability. Contribution of Working Group II to the Fourth Assessment Report of the Intergovernmental Panel

on Climate Change, ML Parry, OF Canziani, JP Palutikof, PJ van der Linden, CE Hanson, Eds., Cambridge University Press, Cambridge UK, 433-467.

Christensen OB, Drews M, Christensen JH (2006). The DMI-HIRHAM regional climate model version 5. Denmark: DMI Tech. Rep. 06-17.

Colen L, Demont M, Swinnen J (2013). Smallholder participation in value chains: The case of domestic rice in Senegal.In: Rebuilding West Africa's Food Potential, Elbehri A. (ed.), FAO/IFAD, 391-415.

Climate-Smart Agriculture in Senegal (2016). Economic relevance of agriculture in Senegal.

Diallo I, Giorgi F, Deme A, Tall M, Mariotti L, Gaye AT (2016). Projected changes of summer monsoon extremes and hydroclimatic regimes over West Africa for the twenty-first century. Clim. Dyn. 47(12):3931-3954

Diallo I, Sylla MB, Giorgi F, Gaye AT, Camara M (2012). Multi-model GCM-RCM ensemble based projections of temperature and precipitation over West Africa for the early 21st century. Int. J. Geophys. 2012(972896):19.

FAO (2014). Sécurité Alimentaire et Implications Humanitaires en Afrique de l'Ouest et au Sahel. N°55, Note Conjointe *FAO-PAM*.

FAO (2016). FAOSTAT Senegal. Available at: http://faostat3.fao.org/home/E.

Giorgi F, Jones C, Asrar G (2009). Addressing climate information needs at the regional level. The CORDEX framework. WMO Bulletin, July 2009 issue.

Giorgi F, Coppola E, Raffael F, Diro GT, Fuentes-Franco R, Giuliani G, Mamgain A, Llopart MP, Mariotti L, Torma C (2014). Changes in extremes and hydroclimate regimes in the CREMA ensemble projections. Abdus Salam International Centre for Theoretical Physics. Trieste. Italy. Clim. Change DOI 10.1007/s10584-014-1117-0.

Hawkins Ed, Osborne TM, Ho CK, Challinor AJ (2012). Calibration and bias correction of climate projections for crop modelling: an idealised case study over Europe. Ag. For. Met. DOI: 10.1016/j.agrformet.2012.04.007

International Benchmark Sites Network for Agrotechnology Transfer (1993). The IBSNAT Decade. Department of Agronomy and Soil Science, College of Tropical Agriculture and Human Resources, University of Hawaii, Honoluly, Hawaii.

IPCC (2013). Climate Change (2013): The Physical Science Basis. In T. F. Stocker, D. Qin, G. -K.Plattner, M. Tignor, S. K. Allen, J. Boschung, A. Nauels, Y. Xia, V. Bex and P. M. Midgley (Eds.), Contribution of Working Group I to the Fifth Assessment Report of the Intergovernmental Panel on Climate Change (p. 1535). Cambridge, United Kingdom and New York, NY, USA: Cambridge University Press. doi:10.1017/CBO9781107415324.

Jones RJ, Ouattar S, Crookston RK (1984). Thermal environment during endosperm cell division and grain filling in maize: Effects on kernel growth and development in vitro. Crop Sci. 24:133–137.

Jones JW, Tsuji GY, Hoogenboom G, Hunt LA, Thornton PK, Wilkens PW, Imamura DT, Bowen WT, Singh U (1998). Decision support system for agrotechnology transfer: DSSAT v3. in Understanding Options for Agricultural Production, eds Tsuji GY, Hoogenboom G, and Thornton PK, Kluwer Academic Publishers. Dordrecht, pp. 129-156. ISBN0-7923-4833-8.

Kouadio AL (2007). Des Interuniversitaires en gestion des risques naturels : Prévision de la production nationale d'arachide au Sénégal à partir du modèle agrométéorologique AMS et du NDVI. ULG-Gembloux 54 p.

Kotir JH (2010). Climate change and variability in Sub-Saharan Africa: a review of current and future trends and impacts on agriculture and food security. Environ. Dev. Sustain. 13:587–605.

Klutse NAB, Sylla MB, Diallo I, Sarr A, Dosio A, Diedhiou A, Kamga A, Lamptey B, Ali A, Gbobaniyi OG, Owusu K, Lennard C, Hewitson B, Nikulin G, Panitz HJ, Buchenf M (2015). Daily Characteristics of West African Summer Monsoon Precipitation in CORDEX Simulations. Theor. Appl. Climatol. DOI 10.1007/s00704-014-1352-3.

Kouakou KE, Koudio ZA, Kouassi FW, Bi TAG, Savane I (2014). Modélisation de la température et de la pluviométrie dans un contexte de changement climatique : cas de l'Afrique de l'Ouest. Afr. Sci. 10(1):145-160.

Mbaye I (2016). Manifestations et stratégies d'adaptation au

changement climatique: des indicateurs opérationnels pour la gouvernance de la ville de Ziguinchor (Sénégal). Vol 1(6) Nouvelle Série, Sciences humaines.

Mariotti L, Coppola E, Sylla MB, Giorgi F, Piani C (2011). Regional climate model simulation of projected 21st century climate change over an all-Africa domain: comparison analysis of nested and driving model results. J. Geophys. Res. 116:22.

Moss RH, Edmonds JA, Hibbard KA, Manning MR, Rose SK, van Vuuren DP, Carter TR, Emori S, Kainuma M, Kram T, Meehl GA, Mitchell JF, Nakicenovic N, Riahi K, Smith SJ, Stouffer RJ, Thomson AM, Weyant JP, Wilbanks TJ (2010). The next generation of scenarios for climate change research and assessment. Nature 463:747-756.

M'Po YN, Lawin AE, Oyerinde GT, Yao BK, Afouda AA (2016). Comparison of Daily Precipitation Bias Correction Methods Based on Four Regional Climate Model Outputs in Ouémé Basin, Benin. Hydrology 4(6):58-71.

Msongaleli B, Rwehumbiza F, Tumbo SD, Kihupi N (2014). Sorghum Yield Response to Changing Climatic Conditions in Semi-Arid Central Tanzania: Evaluating Crop Simulation Model Applicability. Agric. Sci. 5:822-833.

Nikulin G, Jones C, Giorgi F, Asrar G, Büchner M, Cerezo-Mota R, Christensen OB, Déqué M, Fernandez J, Hänsler A, van Meijgaard E, Samuelsson P, Sylla MB, Sushama L (2012). Precipitation climatology in an ensemble of CORDEX-Africa regional climate simulations. J. Clim. 25:6057-6078.

Noba K, Ngom A, Guèye M, Bassène C, Kane M, Diop I, Ndoye F, Mbaye MS, Kane A, Ba AT (2014). L'arachide au Sénégal : état des lieux, contraintes et perspectives pour la relance de la filière. OCL. doi:10.1051/ocl/2013039.

Paeth H, Hall NM, Gaertner MA, Alonso MD, Moumouni S, Polcher J, Ruti PM, Fink AH, Gosset M, Lebel T, Gaye AT, Rowell DP, Moufouma-Okia W, Jacob D, Rockel B, Giorgi F, Rummukainen M (2011). Progress in regional downscaling of West African precipitation. Atmos. Sci. Lett. 12(1):75-82.

Potop V, Mateescu E, Türkott L, Zahradníček P, Boroneanţ C, Constantinescu F, Iamandei M (2014). Application of DSSAT model to simulated thermophilic crops in central and southern Europe. Rožnovský, J., Litschmann, T., (eds): Mendel a bioklimatologie. Brno, 3-5. 9. 2014, ISBN 978-80-210-6983-1.

Rezzoug W, Gabrielle B (2015). Simulation of climate change impact on wheat production in the Tiaret region of Algeria using DSSAT model. Eur. Sci. J. 11:9.

Salack S, Muller B, Gaye AT (2011). Rain-based factors of high agricultural impacts over Senegal. Part I: integration of local to sub-regional trends and variability. Theor. Appl. Climatol. 106:1-22.

Salack S, Sarr B, Sangare SK, Ly M, Sanda IS, Kunstmann H (2015). Crop-climate ensemble scenarios to improve risk assessment and resilience in the semi-arid regions of West Africa. Clim. Res. 65:107-121.

Samuelsson P, Jones CG, Willen U, Ullerstig A, Gollvik S, Hansson U, Jansson C, Kjellstrom E, Nikulin G, Wyser K (2011). The Rossby centre regional climate model RCA3: model description and performance. Tellus A 63:4-23.

Sarr AB, Camara M (2017). Evolution des indices pluviométriques extrêmes par l'analyse de modèles climatiques régionaux du programme CORDEX: Les projections climatiques sur le Sénégal. Eur. Sci. J. 13(17).

Sylla MB, Nikiema PM, Gibba P, Kebe I, Klutse NAB (2016). Climate Change over West Africa: Recent Trends and Future Projections. J.A. Yaro and J. Hesselberg (eds.). Adaptation to Climate Change and Variability in Rural West Africa. DOI 10.1007/978-3-319-31499-0_3.

van Meijgaard E, van Ulft L, van de Berg WJ, Bosveld FC, van den Hurk B, Lenderink G, Siebesma AP (2008). The KNMI regional atmospheric climate model RACMO version 2.1, Tech. Rep. 302.

Waha K, Huth N, Carberry P, Wang E (2015). How model and input uncertainty impact maize yield simulations in West Africa. Environ. Res. Lett. 10(2015):024017.

Related Journals:

African Journal of
Pure and Applied Chemistry

Journal of
Environmental Chemistry and Ecotoxicology

Journal of
Geology and Mining Research

Journal of
Internet and Information Systems

Journal of
Oceanography and Marine Science

Journal of
Petroleum Technology and Alternative Fuels

Journal of
Agricultural Biotechnology and Sustainable Development

International Journal of
Physical Sciences

Scientific Research and Essays

academicJournals

www.academicjournals.org